

## Control of population and entanglement of two qubits under the action of different types of dissipative noise

G. J. Delben <sup>1</sup>, A. L. O. dos Santos <sup>2</sup> and M. G. E. da Luz <sup>2</sup>

<sup>1</sup>*Departamento de Ciências Naturais e Sociais, Universidade Federal de Santa Catarina, Caixa Postal 101, 89520-000 Curitiba-Santa Catarina, Brazil*

<sup>2</sup>*Departamento de Física, Universidade Federal do Paraná, Caixa Postal, 19044, 81531-980 Curitiba-Paraná, Brazil*



(Received 2 April 2022; accepted 5 August 2022; published 19 August 2022)

We investigate the quantum control of two qubits interacting with a Markovian environment and evolving as an  $X$  state. The control is implemented via a simple applied field, whose profile is determined by means of the piecewise time-independent quantum control method. The goal is to make either the population or the system concurrence to follow a specified tracking control trajectory. By considering the system under the influence of three kinds of noise—phase damping, amplitude damping, or a combination of both—we unveil the conditions (like energy balance) under which the quantum control is properly achieved and fidelity (monitored through the trace distance) is kept satisfactorily high, even if the qubits interact differently with the dissipative medium. We further find that the effects of phase damping, a type of noise which notoriously destroys coherence and entanglement, can be mitigated if during the control the system is also exposed to amplitude damping. Of potential interest for the usage of entanglement as resource for quantum information, our results indicate that distinct entanglement measures and coherence can be maintained relatively high (even at long times) as a consequence of the tracking quantum control process.

DOI: [10.1103/PhysRevA.106.022417](https://doi.org/10.1103/PhysRevA.106.022417)

### I. INTRODUCTION

Entanglement is certainly one of the most intriguing aspects of quantum mechanics, deeply related to its nonlocality and a type of correlation without a classical counterpart. Among potential applications, entanglement is a fundamental resource for quantum information and computation [1,2]. In fact, it is essential in areas like teleportation, quantum communication, qubit error correction, superdense coding, quantum networks, etc. [3–9]. In a system completely uncoupled to the surroundings, entanglement remains conserved under any local unitary transformation and can change only through nonlocal evolution. Thus, closed systems are ideal for quantum information tasks. However, total isolation is a rarity in the natural world [3]. Actual quantum systems are usually exposed to the external environment and hence to (Markovian or non-Markovian) stochastic interactions. In this way, we do not have a pure unitary evolution and some information loss might take place [10]. This can be a major problem for such systems functioning as quantum processors, for example.

Therefore, realistically one often begins with a quantum state (described by a density matrix  $\rho$ ), which along time does evolve subjected to a certain degree of decoherence due to the environment. Mathematically (details in the next sections), decoherence corresponds to a tendency of the off-diagonal terms of  $\rho(t)$  to vanish, with the quantum system then resembling (but not being exactly to, Ref. [11]) a statistical ensemble of states, moreover losing its quantum interference characteristics as the  $\rho_{nm}(t)$ 's ( $n \neq m$ ) go to zero. Thus, the common concerns are (i) how to initially create an open quantum systems state with a desirable level of entanglement [12]

(corresponding to proper values for the  $\rho_{nm}(0)$ 's) and (ii) how to handle the system plus environment, so to maintain as long as possible the entanglement [13].

The point (i) relates to state preparation techniques, e.g., as to generate  $X$  states (Sec. II), not being our focus here. But regarding (ii), quantum control (QC) may be a useful solution. Briefly [14], to control a quantum system means to apply an external time-tunable potential  $V(t)$ , basically a laser field, so to induce a predetermined dynamics for it. For instance, a properly chosen laser field could make a given expected value of an observable  $\mathcal{O}$ —namely,  $\langle \mathcal{O} \rangle(t) = \text{Tr}[\rho(t)\mathcal{O}]$  for  $\text{Tr}[A]$  the trace of  $A$ —to follow a desired target trajectory  $S(t)$ . This is known as tracking QC. Observe that driving the problem evolution through a well-tailored  $V(t)$  is basically what one should do to execute quantum computation protocols [15], say, manipulating states in a quantum gate, processing information stored in quantum memories, performing quantum metrology, etc. The distinction (and advantage) is that the QC conceivably would also be a way to overcome the decoherence and dissipation conundrums in open quantum systems.

Although some procedures based on QC have already been tested to suppress (or at least to fairly delay) the loss of entanglement [16–19], a key issue is that QC is much easier to perform and far more developed for closed than for open systems [20]. Furthermore, certain unresolved conceptual aspects can pose difficulties for the proper usage of QC techniques. For instance, both coherence and entanglement are associated to the same basic characteristic, quantum superposition, but how exactly these two phenomena quantitatively associate to each other is still not fully understood [21]. Such

a lack of knowledge makes it hard to explain why certain QC protocols targeting to preserve coherence can lead to a diminishing of entanglement [3]. Also, it is not clear why increasing the intensity of an applied laser field—to speed up the dynamics toward the control—yields a rapid decrease of entanglement [3].

The panorama is not different for the control of entanglement in qubits, a problem extensively discussed in the literature given its practical relevance [22–34]. There are still many open questions regarding this sort of control [20]. For instance, even for a single qubit (essentially a two-level system) there are important points regarding how dephasing and non-Markovian thermal effects may hinder population inversion through QC [35–37]. Concerning the (indirect) interaction between the control field and the environment, these include how the energy injected into the system by the field dissipates into the environment and how this energy flow affects the system degree of entanglement (among the few works addressing these queries, we mention Refs. [6,12,38]). In fact, to answer these and other issues it is very important to adequately typify the exact nature of the dissipative coupling to the environment. The two main causes for a decay in the amount of entanglement in concrete open systems—and common in the implementation of quantum communication protocols—are the so called *amplitude damping* (AD), responsible for a direct energy dissipation, and the *phase damping* (PD), which utterly drives to zero the density matrix elements responsible for the system coherence [10,39–41].

In this work, we suppose two coupled qubits evolving in a X state (a useful configuration in the study of multipartite entanglement [42]) under the influence of the aforementioned AD and PD noises. We discuss the dynamical evolution and the entanglement “degradation” [43] of such open quantum system, computing the time dependence of relevant quantities as energy expected values and coherence degree. To quantify entanglement, we consider two of its most widely used measures, concurrence and negativity. When analyzing the possibility of distinct couplings of the qubits to the noise source, we also calculate the trace distance, linked to the idea of quantum fidelity.

We propose to stabilize and preserve entanglement and coherence for relatively longer times via tracking QC [44], an approach not usually employed in open composed systems (exactly our case here). To do so, we use the piecewise time-independent quantum control method [45,46], a framework already applied with success to open systems [47]. The main quantities we shall control are the population and the entanglement measure concurrence. We find that even under the presence of AD and PD noises, the method leads to a high fidelity control, i.e., the behavior of both qubits are similar and accurately driven (crucial in any implementation of quantum information processing and computation [48,49]). Further, although the combination of distinct types of noise has already been investigated in the literature [50], we show somehow surprisingly that the AD may be used to maintain decoherence when the system is also under the action of the PD noise. By monitoring central features of the system (e.g., the energy dissipation), we are able to infer relevant aspects on the limits of QC protocol, like the effects of the PD interaction

on the system energy and how decoherence and energy loss are related.

The paper is organized as the following. In Sec. II, we introduce our system as well as the main equations representing the coupling of the qubits to a Markovian environment with different kinds of noise. In Sec. III, we outline the QC protocol to be used for the problem. In Sec. IV, we present all our results. Finally, in Sec. V pertinent discussions and a conclusion are given. A short review about measures for entanglement and coherence considered in this work is left to an Appendix.

## II. THE SYSTEM

Whenever necessary, we assume the order convention  $|ab\rangle = |a_1\rangle \otimes |b_2\rangle$  and  $C = A \otimes B = A_1 \otimes B_2$ . So, unambiguously we can drop any subscript notation for the qubits  $Q_1$  and  $Q_2$ . Their mutual Hamiltonian reads

$$\frac{H_0}{\hbar\omega_0} = \frac{\alpha_1}{2}\sigma_z \otimes I + \frac{\alpha_2}{2}I \otimes \sigma_z + \gamma[\sigma_+ \otimes \sigma_- + \sigma_- \otimes \sigma_+]. \quad (1)$$

In Eq. (1),  $\omega_n = \alpha_n \omega_0$  is the  $Q_n$  transition frequency and the terms within the square brackets describe the interaction (of strength  $\gamma$ ) between the qubits in the rotating wave approximation [51]. The quantities  $\alpha_n$  and  $\gamma$  are dimensionless,  $\sigma_x$ ,  $\sigma_y$ , and  $\sigma_z$  are the usual Pauli matrices, with  $\sigma_{\pm} = (\sigma_x \pm i\sigma_y)/2$  (the factor 1/2 is usual in the quantum information literature [52]), and  $I$  is the identity operator. For an isolated  $Q_n$ , the fundamental and excited states are represented by  $|g\rangle$  and  $|e\rangle$ . Then, for the particular case of  $\alpha_1 = \alpha_2 = \alpha$ , the four eigenstates and eigenenergies of  $H_0/(\hbar\omega_0)$  are

$$\{|g g\rangle; -\alpha\rangle, \quad \{|e e\rangle; +\alpha\rangle, \quad \left\{ \frac{1}{\sqrt{2}}(|g e\rangle \pm |e g\rangle); \pm\gamma \right\}. \quad (2)$$

Next, we assume an external potential  $U$  for the system, such that the problem Hamiltonian becomes  $H_s = H_0 + U$ . As we are going to see in Sec. III, the quantum control is implemented through a properly tailored temporal dependence for  $U$ . For sake of discussion, below we suppose  $U$  to be time independent.

As usual (see, e.g., Ref. [51]), we can take a single external potential for both  $Q_n$ 's; namely, we do not need to consider two independent fields, each acting just on one qubit. Thus, motivated by Ref. [53], we set  $U/(\hbar\omega_0) = V \otimes \sigma_x$ , which is a very common interaction assumed between two qubits [54,55]. As the implementation of the QC is concerned, after numerical tests we have verified that there is no relevant advantage in supposing the external potential as  $V \otimes \sigma_y$  or more generally as  $V \otimes (c\sigma_x + d\sigma_y)$  (we observe that  $V \otimes \sigma_z$  represents an ineffective coupling). So, our results here are already representative of typical situations for the coupling of two qubits in the context of quantum information.

The dimensionless  $V$  is parameterized as (see Sec. III)

$$V = \lambda \begin{pmatrix} 0 & \exp[-i\phi] \\ \exp[i\phi] & 0 \end{pmatrix}. \quad (3)$$

For  $\alpha_1 = \alpha_2 = \alpha$ , the four eigenstates and eigenvalues of  $H_s/(\hbar\omega_0)$  are ( $a = \lambda/\alpha$ ,  $b = \lambda/\gamma$ )

$$\left\{ |F^{(\pm)}\rangle = A^{(\pm)} |g g\rangle \pm B^{(\pm)} |e e\rangle; \pm\alpha\sqrt{1+a^2}, \quad \left\{ \frac{1}{\sqrt{2}}(|g e\rangle \pm D |e g\rangle); \pm\gamma\sqrt{1+b^2+2b\cos[\phi]} \right\}, \right.$$

$$f = \frac{1}{\sqrt{2(1+a^2+\sqrt{1+a^2})}}, \quad B^{(+)} = A^{(-)} = \frac{1+\sqrt{1+a^2}}{f}, \quad A^{(+)} \exp[-i\phi] = B^{(-)} \exp[+i\phi] = \frac{a}{f},$$

$$D = \frac{\sqrt{1+b^2+2b\cos[\phi]}}{1+b\exp[i\phi]}, \quad (4)$$

which, as it should be, reduces to Eq. (2) for  $\lambda = 0$ .

A common formalism to treat a Hamiltonian  $H_s = H_0 + U$  interacting with the environment (assuming a Markovian process) is based on complete positive semigroup maps, represented by a Lindblad-like quantum master equation [15,51]. For  $\rho_s(t)$  the system density matrix, one has

$$\frac{\partial}{\partial t} \rho_s(t) = -\frac{i}{\hbar} [H_s, \rho_s(t)] + \mathcal{L}(\rho_s(t)), \quad (5)$$

where  $\mathcal{L}$  is the superoperator coupling the system to the dissipative media.

The AD noise usually induces energy dissipation from the system to the surroundings [52]. By its turn, the PD noise describes a somehow more subtle process, responsible for the loss of quantum information. Indeed, for any unitary evolution, each energy eigenvector (composing the system full state) accumulates a phase factor, proportional to the corresponding eigenenergy. However, due to environment induced phase damping, these relative phases may be partially or even totally lost. As a consequence, the off-diagonal elements of  $\rho_s$  tend to decay exponentially fast with time [52].

These two distinct classes of damping are incorporated into the Lindblad formalism by writing (with  $\sigma_w^{(1)} = \sigma_w \otimes I$ ,  $\sigma_w^{(2)} = I \otimes \sigma_w$ , and  $\sigma_w$  representing  $\sigma_z$ ,  $\sigma_+$ , or  $\sigma_-$ )

$$\mathcal{L}(\rho_s) = \omega_0 \sum_{n=1}^2 \left\{ \Gamma_n^{(\text{PD})} \frac{1}{2} (\sigma_z^{(n)} \rho_s \sigma_z^{(n)} - \rho_s) + \Gamma_n^{(\text{AD})} \right.$$

$$\left. \times \left( \sigma_-^{(n)} \rho_s \sigma_+^{(n)} - \frac{1}{2} \sigma_+^{(n)} \sigma_-^{(n)} \rho_s - \frac{1}{2} \rho_s \sigma_+^{(n)} \sigma_-^{(n)} \right) \right\}. \quad (6)$$

Note that for convenience we have defined the dissipation constants in terms of  $\omega_0$  and the dimensionless parameters  $\Gamma$ 's.

At this point, two comments about Eq. (6) are in order. First, to model either one or both types of noise acting on the system, we simply suppose  $\mathcal{L}$  as the linear combination of these two contributions. Then, by properly choosing the associated constants  $\Gamma$ 's we can have the different cases of interest (see the beginning of Sec. IV). Second, in the way we define Eq. (6), although each qubit “feels” qualitatively similar baths, the environments in principle are not common. Nonetheless, this construction is very useful, e.g., to analyze the situation in which the  $Q_n$ 's display distinct dissipation rates (as in Sec. IV D). Actually, split-noise environments have been considered to study various effects in coupled qubits [56–61]. Also, we should emphasize that such separa-

tion of the noise environments are possible for  $Q_n$ 's based on solid-state systems (for a nice discussion, see, e.g., Ref. [53]).

We suppose the system described by a  $X$  density matrix (characteristic of several population families [42]). This is a commonly considered situation due to its mathematical simplicity and a rather direct experimental implementation [62–65]. Here, an additional advantage is that such  $\rho_s$  yields simple expressions for the entanglement measures we wish to discuss (concurrence and negativity). For  $\rho_s = \sum_{j,k=1}^4 \rho_{jk} |j\rangle\langle k|$ , with  $|1\rangle = |e e\rangle$ ,  $|2\rangle = |e g\rangle$ ,  $|3\rangle = |g e\rangle$ ,  $|4\rangle = |g g\rangle$ , the  $X$  structure implies that at any time

$$\rho_s = \begin{pmatrix} \rho_{11} & 0 & 0 & \rho_{14} \\ 0 & \rho_{22} & \rho_{23} & 0 \\ 0 & \rho_{32} & \rho_{33} & 0 \\ \rho_{41} & 0 & 0 & \rho_{44} \end{pmatrix}. \quad (7)$$

For our analysis, we need to compute the energies expected values [6] of the coupled qubits alone,  $\varepsilon_0(t)$ , and of the system (qubits plus the external field)  $\varepsilon_s(t)$ . For  $\alpha_1 = \alpha_2 = \alpha$ , they are given by (rescaled by  $\hbar\omega_0$ , so dimensionless)

$$\varepsilon_0(t) = \text{Tr} \left[ \rho_s(t) \frac{H_0}{\hbar\omega_0} \right] = \alpha(\rho_{11}(t) - \rho_{44}(t)) + 2\gamma \text{Re}[\rho_{23}(t)] \quad (8)$$

and

$$\varepsilon_s(t) = \text{Tr} \left[ \rho_s(t) \frac{H_s}{\hbar\omega_0} \right]$$

$$= \varepsilon_0(t) + 2\lambda \text{Re}[\exp[i\phi](\rho_{14}(t) + \rho_{23}(t))]. \quad (9)$$

Lastly, for our purposes in the present contribution we shall address measures of quantum coherence ( $C$ ) and entanglement, in particular, concurrence ( $E_C$ ), negativity ( $E_N$ ), and trace distance ( $T_D$ ). All them are discussed and proper expressions are given in Appendix.

### III. THE QUANTUM CONTROL SCHEME

Tracking QC can be summarized as the following. For an observable represented by the operator  $\mathcal{O}$  and a given initial  $\rho(0)$ , the goal is to find a proper time-dependent external potential  $U(t)$  such that the evolved  $\rho(t)$  should, for any  $0 \leq t \leq T$ , lead to

$$\langle \mathcal{O} \rangle(t) = \text{Tr}[\rho(t) \mathcal{O}] = S(t). \quad (10)$$

The function  $S(t)$  is the aimed (i.e., previously specified) QC target trajectory. Hence, the time evolution of the expected value of  $\mathcal{O}$  would be established from the way a chosen laser field profile [yielding  $U(t)$ ] drives the system.

With this purpose, we consider the piecewise time-independent quantum control method (PTIQCM), conceptually a very simple approach [45]. One divides the whole time interval of interest into  $M$  temporal windows  $\delta t_m$ —usually all equal, so that  $\delta t_m = \delta t = T/M$  for  $m = 1, 2, \dots, M$ . One then sets instants  $t_m$  as the middle of the interval  $\delta t_m$ . The PTIQCM main idea is to look for time-independent potentials  $V_m$ 's within  $t_m - \delta t/2 < t < t_m + \delta t/2$ , resulting in  $\text{Tr}[\rho(t_m)\mathcal{O}] = S(t_m)$ . Now, if (i) the external laser field parameters can be tuned in such way that the switching  $V_m \rightarrow V_{m+1}$  is fast (compared to  $\delta t$ ) and (ii)  $\delta t$  is sufficiently short, the obtained  $\langle \mathcal{O} \rangle(t)$  from these successive  $V_m$ 's is a good approximation for Eq. (10). In fact, as discussed and exemplified in Refs. [46,47], the conditions (i) and (ii) are very feasible from present-day laser sources technology. Therefore, for a certain  $S(t)$  the PTIQCM determines the laser “shape”  $\{V_1, V_2, \dots, V_M\}$  ensuring the desired expected value of  $\mathcal{O}$  as function of time.

Within each  $\delta t_m$ , we assume that the  $V_m$  results from an external harmonic monochromatic electric field in the dipolar approximation (details about using such type of potential for the control of qubits can be found, e.g., in Refs. [47,54,66]). Thus, in the unperturbed single-qubit basis we can parameterize

$$V_m = -\Omega_{R,m} \begin{pmatrix} 0 & \exp[-i\varphi_m] \\ \exp[i\varphi_m] & 0 \end{pmatrix}, \quad (11)$$

where  $\Omega_R$  is a dimensionless Rabi frequency (i.e., a product of the modulus of the applied field by the system dipole moment divided by  $\hbar\omega_0$ ) and  $\varphi$  is the relative phase between the field and the dipole moment vectors. The main diagonal has null elements since the nonperturbed states have, as usually, opposite parities. We note that in each time interval  $\delta t_m$  the parameters  $\Omega_{R,m}$  and  $\varphi_m$  correspond, respectively, to  $-\lambda$  and  $\phi$  in Eq. (3)—the minus signal in Eq. (11) is just a convention [47]. In all the examples in this work, for any  $m$  we assume  $\varphi_m$  to be the same constant. Then, the only effective control parameter will be  $\Omega_R$ . Moreover, unless otherwise explicitly indicated such constant will be set to zero.

An important aspect we would like to emphasize is that as in any typical inverse problem scheme, we do not have just an unique tracking QC solution from the PTIQCM [45]. Distinct parameters values for  $V_m$  can lead to  $|\text{Tr}[\rho(t_m)\mathcal{O}] - S(t_m)| < \Delta$  (for the actual computations we take  $\Delta = 10^{-4}$ ). In our numerical algorithm, we “probe” the parameters space, searching for those values satisfying this inequality. Then, we select the ones leading to the lower amplitudes and smoother field profiles. As we are going to see, these constraints may be hard to meet if the control conditions are more demanding.

For the  $X$  population structure of  $\rho(t)$ , Eq. (7), and for a generic  $\mathcal{O}$  operator represented by a  $4 \times 4$  Hermitian matrix, we have

$$\begin{aligned} \langle \mathcal{O} \rangle &= \rho_{11} \mathcal{O}_{11} + \rho_{22} \mathcal{O}_{22} + \rho_{33} \mathcal{O}_{33} + \rho_{44} \mathcal{O}_{44} \\ &+ (\rho_{14} + \rho_{41}) \mathcal{O}_{14} + (\rho_{23} + \rho_{32}) \mathcal{O}_{23}. \end{aligned} \quad (12)$$

All the measures mentioned in the previous section as well as the system population can be written as the above expression. So, for a certain  $S(t)$  we consider  $\langle \mathcal{O}(t) \rangle = S(t)$  with  $\langle \mathcal{O}(t) \rangle$  given by Eq. (12) and then employ the PTIQCM to determine the sought QC [54].

Finally, we mention that the general computational prescriptions (and details about field parameters optimization) for the PTIQCM are presented in Ref. [46]. Also, its specific implementation to the Lindblad quantum master equation is explained in length in Ref. [47]. Further, more technically and computationally oriented works about the PTIQCM applied to open quantum systems can be found in Refs. [54,66].

#### IV. RESULTS

In all of the following, the analyzed quantities are dimensionless. Indeed, for the energies, see Eqs. (8) and (9), and for coherence and entanglement measures, see the Appendix. Also, time is given in units of  $\omega_0^{-1}$ , so that we consider the dimensionless  $\tau = \omega_0 t$ . For the numerics, we always set  $\alpha_1 = \alpha_2 = \gamma = 1.0$  and unless in Sec. IV D, we assume a same environment coupling for both qubits, thus  $\Gamma_1 = \Gamma_2$  (in this case leading to a high fidelity for the populations). For a pure amplitude (phase) damping AD (PD) noise,  $\Gamma^{(\text{AD})} = \Gamma$  and  $\Gamma^{(\text{AD})} = 0$  ( $\Gamma^{(\text{AD})} = \Gamma$  and  $\Gamma^{(\text{PD})} = 0$ ). If both dampings take place, then  $\Gamma^{(\text{AD})} = \Gamma^{(\text{PD})} = \Gamma$  (the APD noise). Here  $\Gamma = 0.1$ . For the time windows, we suppose  $M = 1000$  intervals for any discussed  $T$  (Sec. III). For a  $X$  coupling structure, Eq. (7), we need to show only the density matrix elements  $\rho_{jj}$  (with  $j = 1, 2, 3, 4$ ),  $|\rho_{14}|$ , and  $|\rho_{23}|$  (obviously,  $\rho_{41} = \rho_{14}^*$  and  $\rho_{32} = \rho_{23}^*$ ). All the others are null during the entire time evolution.

Before addressing the instances with external applied fields, it is instructive to briefly illustrate the case where only the environment interacts with the qubits [so  $V = 0$  and  $\varepsilon_0(\tau) = \varepsilon_s(\tau)$ ]. As a first example, suppose  $\rho(0) = |e e\rangle\langle e e| = |1\rangle\langle 1|$ . Recall that  $|e e\rangle = |1\rangle$  is an eigenstate of  $H_0$ . The  $\rho_{jk}(\tau)$ 's and energy are depicted in Fig. 1. Note that for any time,  $\rho_{14} = \rho_{23} = 0$ . For the PD noise, the density matrix remains stationary, namely,  $\rho(\tau) = \rho_{11}(\tau) = 1$ . Thus, the system energy  $\varepsilon_s(\tau) = 1$  does not change. On the other hand, the AD noise drives the system toward the ground state, i.e.,  $\rho_{44} \rightarrow 1$  with all other  $\rho_{jj}$  vanishing, consequently  $\varepsilon_s \rightarrow -1$ . This trend is also observed for APD. Actually, AD and APD display the exact same behavior since in the current situation the extra phase damping in APD does not influence the dynamics (see the plots for PD in Fig. 1). Lastly, the measures of coherence and entanglement are always zero.

As a second example, at  $\tau = 0$  we suppose all the non-null elements in Eq. (7) equal to  $1/4$ . The results are shown in Fig. 2, where for any noise type  $\rho_{14}, \rho_{23} \rightarrow 0$ . The diagonal terms  $\rho_{jj}$  ( $j = 1, 2, 3, 4$ ) remain unaltered for PD, so that  $\varepsilon_s \rightarrow 0$ , i.e., the system tends to a simple average over the eigenenergies  $+1$  and  $-1$ . Conversely, for AD and APD  $\rho_{44} \rightarrow 1$  with the other  $\rho_{jj}$ 's vanishing. The corresponding negativity  $E_N$  and coherence  $C$  are shown in Fig. 3; they do go to zero with time. The concurrence  $E_C$ , not shown, is always zero.

Next we discuss the system dynamics under external applied fields. Unless otherwise explicitly mentioned, at  $\tau = 0$  we will take

$$\rho(0) = |\psi_0\rangle\langle\psi_0| = |g g\rangle\langle g g| = |4\rangle\langle 4|. \quad (13)$$

Thus, initially only the matrix element  $\rho_{44} = 1$  is not null, the system is not entangled and  $\varepsilon_0(0) = -\alpha = -1$ . This  $|\psi_0\rangle$  is

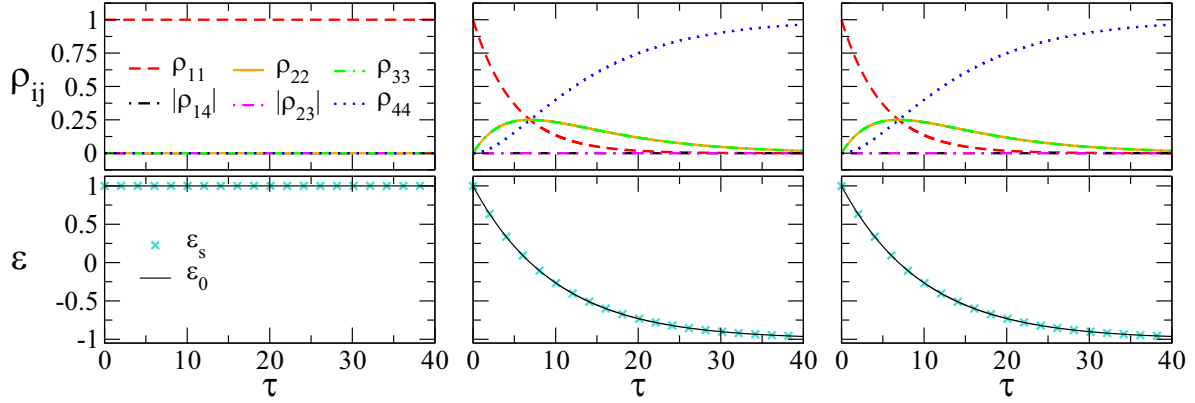


FIG. 1. In the absence of an external applied field, the temporal evolution of both  $\rho$  and the expected value of the system energy  $\varepsilon_s = \varepsilon_0$ . Each column represents one type of environment noise: first, second, and third, respectively, PD, AD, and APD. Here all  $\rho_{jk}(0) = 0$  unless for  $\rho_{11}(0) = 1$ . Thus, initially both qubits are in the excited state with  $\varepsilon_s(0) = 1$ .

the ground state of  $H_0$ . Regarding QC of entanglement, this is a challenging choice for  $\rho(0)$  since in the absence of an external field, the concurrence should remain zero at any time. Further, for  $|F^{(\pm)}\rangle$  two of the four possible eigenstates of the qubits interacting with a constant field and no noise, Eq. (4), we have

$$|g g\rangle = f^{-1} ((1 + \sqrt{1 + a^2}) |F^{(-)}\rangle + a \exp[-i\phi] |F^{(+)}\rangle). \quad (14)$$

So, for  $\alpha_1 = \alpha_2 = \alpha$ , the initial state given by Eqs. (13) and (14) and a constant field, if there was no coupling to the environment, one would get  $\varepsilon_s(t) = -\alpha$  (so a constant) and  $\varepsilon_0(t)$  following simple harmonic oscillations within the amplitude interval  $[-\alpha, \alpha(a^2 - 1)/(a^2 + 1)]$ .

### A. The system with a fixed external applied field

We start considering the qubits plus environment and a fixed external applied field, without any attempt of a quantum control. We assume a typical situation with  $\varphi_m = \varphi = 0$  and  $\Omega_{R,m} = \Omega_R = 1$  [see Eq. (11) and recall that  $\Omega_R$  is given in units of  $\omega_0$ ]. The results are displayed in Fig. 4. Notice from Figs. 4(a)–4(c) that only for the PD  $\rho$  tends to a 50:50%

mixture with  $\rho_{44}(\tau) = \rho_{11}(\tau) = 1/2$  with the other  $\rho_{jk}(\tau)$ 's vanishing. This is expected for a state undergoing strong decoherence. On the other hand, for AD and APD,  $\rho_{44}(\tau)$  evolves toward a constant value  $\tilde{\rho}_{44} < 1$ . Likewise, some of the other  $|\rho_{jk}|$ 's also tend to constant values, but all smaller than  $\tilde{\rho}_{44}$ .

The expected values of the qubits,  $\varepsilon_0$ , and of the system (qubits plus field),  $\varepsilon_s$ , energies—Eqs. (8) and (9)—are shown in Figs. 4(d)–4(f). From the discussion after Eq. (14), we have that in the absence of noise and for the present parameters, we would get  $\varepsilon_s(\tau) = \varepsilon_s(0) = -1$ , with  $\varepsilon_0(\tau)$  oscillating indefinitely between  $-1$  and  $0$  (thus with an average of  $-0.5$ ). As seen in the plots, only for AD we have  $\varepsilon_s(\tau) = -1$  stationary. For the conditions in Fig. 4, for all the noise cases  $\rho_{23}(\tau) = 0$  so that  $\varepsilon_s(\tau) = \rho_{11}(\tau) - \rho_{44}(\tau) - 2\Omega_R \text{Re}[\rho_{14}(\tau)]$ ; see Eqs. (8) and (9). Then, just for AD there is an exact compensation of the variation of  $\rho_{11}(\tau) - \rho_{44}(\tau)$  by that of  $-2\Omega_R \text{Re}[\rho_{14}(\tau)]$ . Moreover, for AD  $\varepsilon_0$  tends to the mean  $-0.5$ , whereas for PD and APD,  $\varepsilon_0$  tends to greater values:  $\varepsilon_s \rightarrow \varepsilon_0 \rightarrow 0$  for PD and  $\varepsilon_0 \rightarrow -0.25, \varepsilon_s \rightarrow -0.5$  for APD. Thence, an important point is that the system energetic trade-off depends on the noise type. Of course, this is a known fact [51], but not well explored in the literature, especially associated to coherence and entanglement (see below).

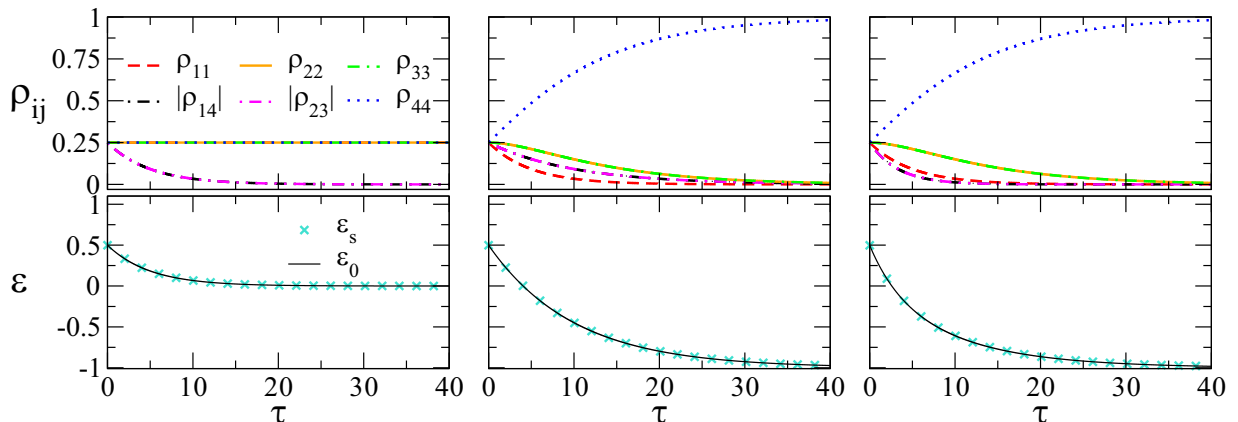


FIG. 2. The same as in Fig. 1, but for all the  $\rho_{jk}(0)$  in the  $X$  structure of Eq. (7) equal to  $1/4$ . Here  $\varepsilon_s(0) = 1/2$ .

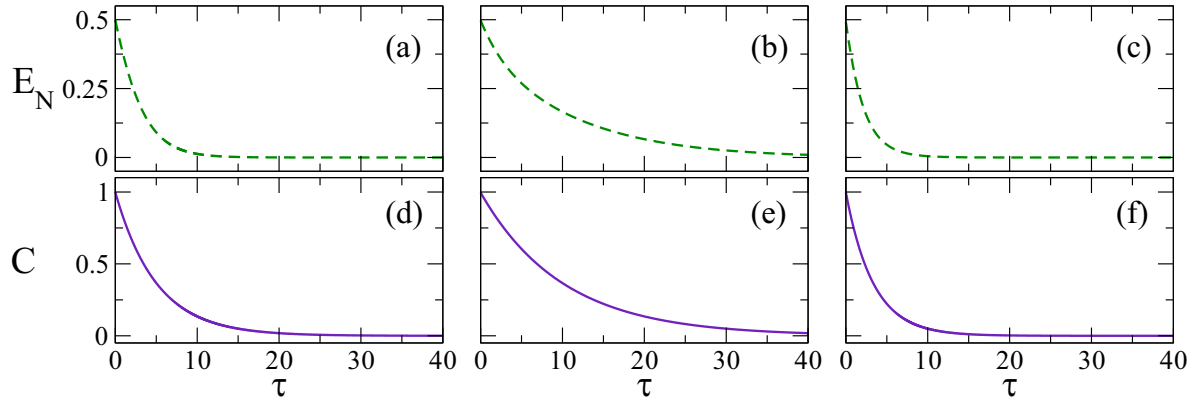


FIG. 3. For the conditions and parameters of Fig. 2, measures of entanglement, negativity  $E_N$ , and coherence  $C$ , see Appendix. All these quantities go to zero, with the AD presenting the slower decay. The first, second, and third columns correspond, respectively, to the PD, AD, and APD noise.

The PD noise asymptotically thermalizes the  $Q_n$ 's in the mixture  $\rho = 1/2(|1\rangle\langle 1| + |4\rangle\langle 4|)$ . This process leads to the observed increasing of energy for the system (now totally “stored” in the qubits degrees of freedom once  $\varepsilon_s \rightarrow \varepsilon_0$ ). On the other hand, the AD usually “drains” the energy from the system. Nonetheless, since we have already started in its fundamental state, Eq. (13), the effect is simply to damp the oscillations of  $\varepsilon_0$  toward its average value. The APD noise shows akin behavior to the previous two, with the final energies being an average of those in PD and AD.

As an extra exploration, we have performed the above same calculations setting  $\rho(0) = |e e\rangle\langle e e| = |1\rangle\langle 1|$ . They are depicted in Fig. 5. Without any coupling to the environment, such  $\rho(0)$  would lead to  $\varepsilon_s(\tau) = +1$  and  $\varepsilon_0(\tau)$  oscillating between 0 and 1. In agreement with our previous observations, Fig. 5 shows that now the thermalization due to the PD decreases the system initial energy, which is also the case for AD and APD. For all the three distinct noises, the limits are exactly those in Fig. 4, namely, for PD  $\varepsilon_s \rightarrow \varepsilon_0 \rightarrow 0$ , for AD  $\varepsilon_s \rightarrow -1$ ,  $\varepsilon_0 \rightarrow -0.5$ , and for APD  $\varepsilon_s \rightarrow -0.5$ ,  $\varepsilon_0 \rightarrow$

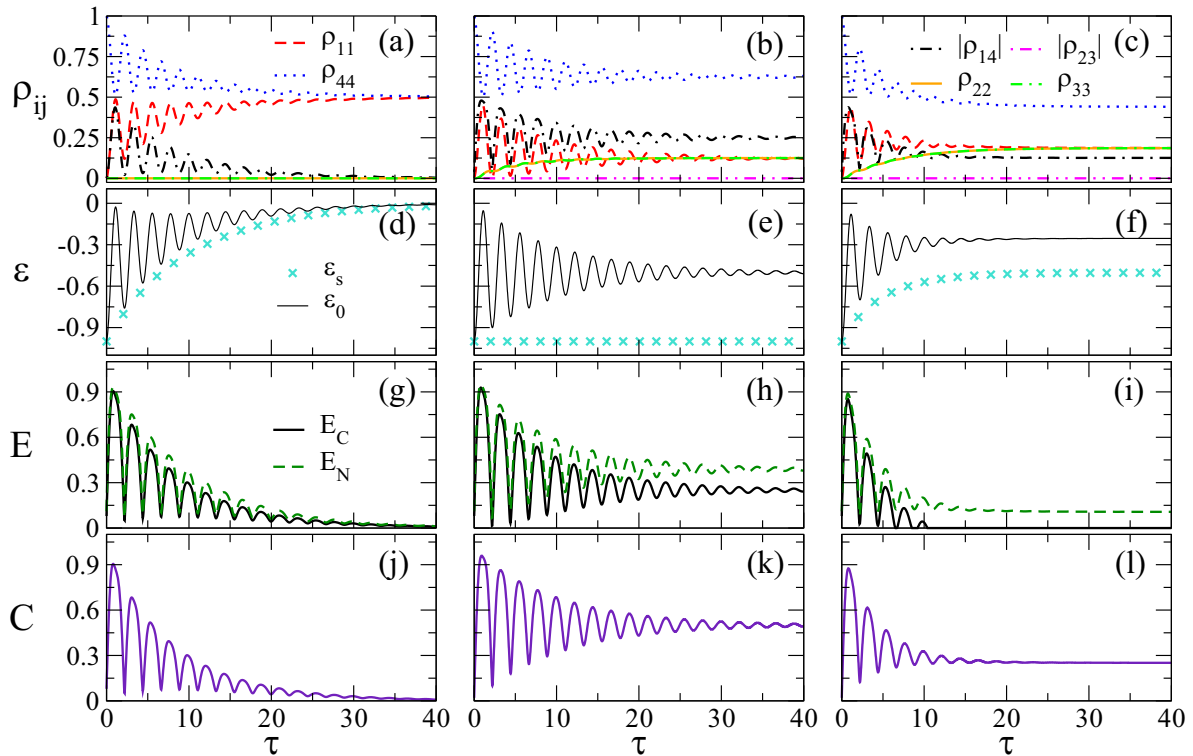


FIG. 4. Assuming a fixed applied field (main text), different quantities as function of the dimensionless time  $\tau$  for  $\rho(0)$  given by Eq. (13). In the first, second, and third columns, the results are shown, respectively, for the PD, AD, and APD noises. [(a)–(c)] The density matrix elements. Always  $\rho_{23} = 0$  and  $\rho_{22} = \rho_{33} = 0$  in panel (a) and  $\rho_{22} = \rho_{33}$  in panels (b) and (c). [(d)–(f)] Energies’ expected values. [(g)–(i)] Entanglement measures: concurrence  $E_C$  and negativity  $E_N$ . [(j)–(l)] The  $l_1$  norm coherence measure  $C$ .

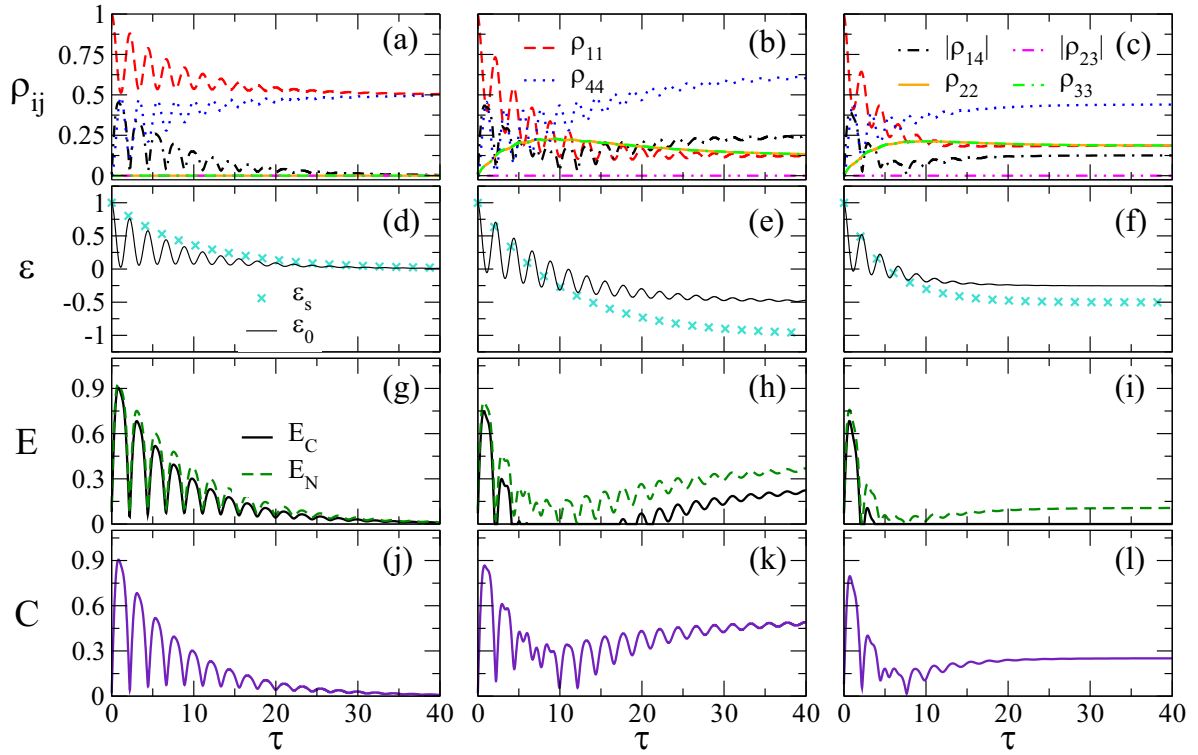


FIG. 5. The same as in Fig. 4, but for  $\rho(0) = |1\rangle\langle 1|$ .

$-0.25$ . These results might seem at odds with  $\varepsilon_s(t) = \varepsilon_0(t) = 1$  for PD in Fig. 1. But the key factor is that there are no applied fields for the dynamics shown in Fig. 1; this obviously influencing the time evolution of the  $\rho_{jk}(\tau)$ 's and thus altering the final energetic balance. For instance, analogously to the corresponding situation in Fig. 4, for PD in Fig. 5,  $\rho_{14}(\tau)$  during a certain time interval is also non-null. This is not observed in Fig. 1.

For a constant applied field, the entanglement measures of concurrence ( $E_C$ ) and negativity ( $E_N$ ) as well as of coherence ( $C$ ) are shown in Figs. 4(g)–4(l) and 5(g)–5(l). Initially they present oscillations with high amplitudes, but then converge to smaller constant values, in some cases considerably smaller. The oscillations in these quantities are just a consequence of the oscillations in the density matrix elements  $\rho_{ij}$ , induced by the applied field. As already reported elsewhere [10,39–41], for PD entanglement and coherence tend to vanish for large enough times, whereas for AD, these quantities tend to an asymptotic stabilization at low values. Nevertheless, when one adds AD to PD (APD noise), even without any QC some entanglement and more emblematic coherence can survive in the system. This points to constructive interference (coherence creation) induced by the external applied field (see, e.g., Refs. [54,67]). In particular,  $E_N(\tau)$  is always greater than zero for AD and APD, a good indication that the field may be able to maintain a certain degree of quantum correlations, implying that decoherence distillation may be possible [13].

### B. Population tracking control

Now we shall implement population tracking QC. For concreteness, we take as our observable expected value  $\langle \mathcal{O} \rangle(\tau) =$

$\rho_{11}(\tau) + \rho_{22}(\tau)$ . Due to the simple properties of the full density matrix, it follows that  $\langle \mathcal{O} \rangle(\tau) = \rho_{ee1}(\tau)$ , which is the  $Q_1$  qubit population in the excited state. As the target trajectory, we propose (already considered in Refs. [46,47,54] with different purposes)

$$S(t) = S_0 \arctan[\tau/\xi], \quad (15)$$

where  $\xi = 10$  and  $0.009 \leq S_0 \leq 0.4$ .

In Figs. 6(a)–6(c), we show the control of  $\rho_{ee1}(\tau)$  in the time range  $0 \leq \tau \leq 40$ ,  $\rho(0)$  given by Eq. (13), the three different kinds of noise and some distinct values for  $S_0$ . From the plots, we see that the QC quality is remarkable, as already mentioned with  $|S(t) - \rho_{ee1}(t)| \leq 10^{-4}$ . Furthermore, in Fig. 6 the only situation in which the control is lost, around  $\tau \approx 30$ , takes place for the parameter value  $S_0 = 0.4$  [cf., Eq. (15)]. In fact, from many other tests—supposing different  $\rho(0)$ 's as well as  $S_0$ 's and  $\xi$ 's in Eq. (15)—we have verified that the control breaks down whenever  $\rho_{ee1}$  approaches 0.5, just the case for  $S(\tau \approx 30) \approx 0.5$  when  $S_0 = 0.4$ .

To better understand the general behavior in Fig. 6, consider all the  $\rho_{ij}(\tau)$  for  $S_0 = 0.32$  in Figs. 6(d)–6(f) and  $S_0 = 0.4$  in Figs. 6(g)–6(i). We first recall that for  $\rho(0)$  in Eq. (13), the system starts in the ground state. Also, since  $\text{Tr}[\rho(\tau)] = 1$ , we have the usual constraint  $\rho_{11} + \rho_{22} + \rho_{33} + \rho_{44} = 1$  for any  $\tau$ . For the PD noise, essentially only  $\rho_{11}$  and  $\rho_{44}$  are non-null, implying that  $\rho_{ee1} = \rho_{11}$ . Further, these two matrix elements evolve toward the mixture  $\rho_{11} = \rho_{44} = 1/2$ . Thence, in this case the QC can be sustained as long as the target trajectory  $S(\tau)$  is not greater than 1/2, a condition verified in Fig. 6(d) for the full time range analyzed, but only for  $\tau \leq 30$  in Fig. 6(g). In turn, the dynamics of the  $\rho_{jk}$ 's is a bit more involved for AD and APD, Figs. 6(e) and 6(h) and

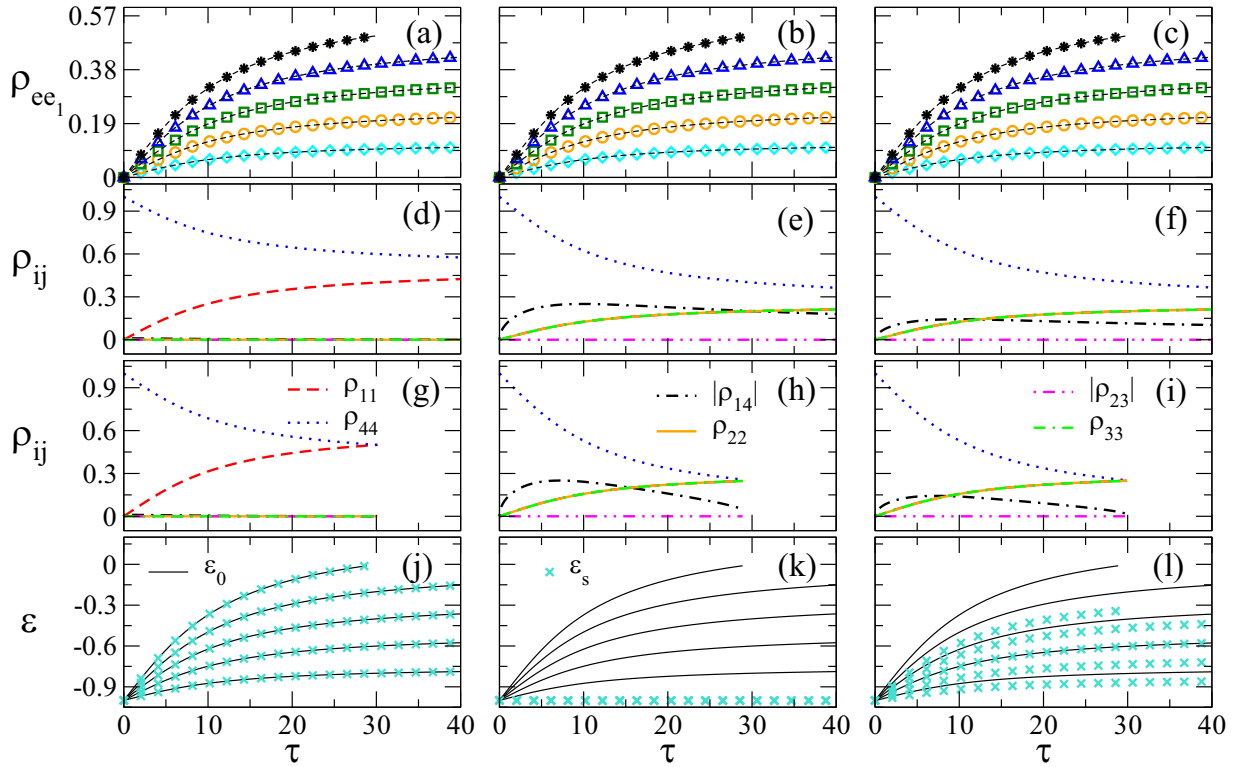


FIG. 6. [(a)–(c)] The obtained tracking QC of  $\rho_{ee_1} = \rho_{11} + \rho_{22}$  (symbols) compared to the aimed target trajectory of Eq. (15) (dashed curves) under the three types of noise, PD, AD, and APD, respectively, in the first, second, and third columns. Here  $\xi = 10$  and the values of  $S_0$  are 0.08 (diamond), 0.16 (circle), 0.24 (square), 0.32 (triangle), and 0.40 (star). The corresponding  $\rho_{jk}(\tau)$  for  $S_0 = 0.32$  (d)–(f) and  $S_0 = 0.4$  (g)–(i). [(j)–(l)] The energies  $\varepsilon_s$  and  $\varepsilon_0$  for the evolution in panels (a)–(c). Exactly like  $\rho_{ee_1}$ , the energies tend to increase with  $S_0$  [so, the relative order of the curves with respect to  $S_0$  is as in panels (a)–(c)]. Note that in panel (j)  $\varepsilon_s$  always coincides with  $\varepsilon_0$  whereas in (k)  $\varepsilon_s = -1$  for all  $S_0$ .

Figs. 6(f) and 6(i). For both noises, as time goes on the innate tendency is  $\rho_{11}$ ,  $\rho_{22}$ , and  $\rho_{33}$  to coincide, but with  $\rho_{44}$  always being greater. So, the tracking QC solution found for the problem results in  $\rho_{11}(\tau) \approx \rho_{22}(\tau) \approx \rho_{33}(\tau)$ ,  $\rho_{ee_1}(\tau) \approx 2\rho_{11}(\tau)$  increasing and  $\rho_{44}(\tau) \approx 1 - 3\rho_{11}(\tau)$  decreasing with  $\tau$  (note that  $\rho_{44}(0) = 1$ ). In this way, the present trajectory control for AD and APD is possible whenever  $\rho_{44} > \rho_{11}$ . This can be sustained for times longer than  $\tau = 40$  if  $S_0 = 0.32$ , and just up to  $\tau = 30$  if  $S_0 = 0.4$  [this latter trend is clearly seen in Figs. 6(h) and 6(i)]. Likewise relevant, the evolution of the qubits energy  $\varepsilon_0(\tau)$  in Fig. 6 also indicates the condition in which the QC strays. Indeed, starting with  $\varepsilon_0(0) = -1$ , the control is lost when  $\varepsilon_0(\tau)$  approaches zero, which is the energy value associated to an equal population of fundamental and excited states for the qubits.

For the QC dynamics in Fig. 6, we display the corresponding entanglement measures of concurrence  $E_C$ , Figs. 7(a)–7(c), and negativity  $E_N$ , Figs. 7(d)–7(f), as well as coherence  $C$ , Figs. 7(g)–7(i). We clearly see that the PD is the worst type of noise to maintain entanglement and coherence. On the other hand, the AD and APD noises lead to similar results, with entanglement and coherence remaining fairly high if  $\rho_{ee_1}$  raises slowly [the case when  $S_0$  in Eq. (15) is small]. Regarding distinctions between concurrence and negativity, overall the population tracking QC can be sustained even if  $E_C$  becomes very low, Figs. 7(a)–7(c). Conversely, at least for AD and APD,  $E_N$  tends to be considerable while the control

takes place, Figs. 7(e)–7(f). So, tracking QC could represent an interesting method for preparing states for entanglement distillation [13].

In Fig. 8, we depict the field profiles resulting in the QC of Fig. 6. In Figs. 8(a)–8(c), the control is attainable in the full time interval and in Figs. 8(d)–8(f), it breaks down around  $\tau \approx 30$ . Note that in Figs. 8(a)–8(c) the field amplitudes vary smoothly, decreasing (increasing) with  $\tau$  for the PD (AD and APD) noise. Such behavior contrasts with that in Figs. 8(d)–8(f). Near the QC collapse, at  $\tau = \tau_{bd}$ , there is a very steep variation of  $\Omega_R$  in an attempt by the method to sustain the control. Actually,  $\Omega_R(\tau \rightarrow \tau_{bd}) \rightarrow \infty$ , meaning that the system would demand infinite energy ( $\sim |\Omega_R|^2$ ) from the field, which of course makes the QC unfeasible.

### C. The tracking control of the concurrence $E_C$

In Sec. IV B, we have seen that although  $E_N$  can be kept relatively high during the population QC, depending on the target trajectory parameters and range of  $\tau$ ,  $E_C$  is more susceptible to a decreasing. Therefore, an important question is if one would be able to control the entanglement measure of concurrence.

To investigate this, we first observe that since  $E_C$  is the maximum between two terms,  $E_{C_1}$  and  $E_{C_2}$  [cf., Eq. (A4)], we can choose one of them to drive the concurrence—of course, maintaining the other small. Thus, we select  $E_{C_2}$ . Second, by

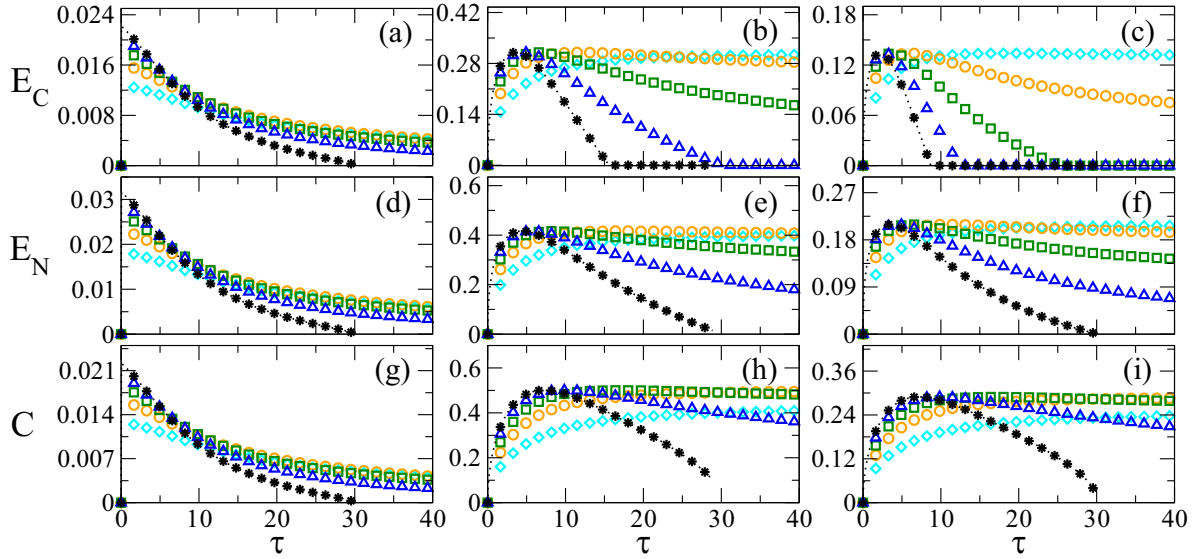


FIG. 7. The resulting entanglement and coherence evolution associated to the population control in Fig. 6. The symbols represent the values of  $S_0$ : 0.08 (diamond), 0.16 (circle), 0.24 (square), 0.32 (triangle), and 0.40 (star). The PD, AD, and APD noise cases are displayed, respectively, in the first, second, and third columns.

examining Eq. (A4), if  $\rho_{11} + \rho_{44}$  is large (so that  $\rho_{22} + \rho_{33} \approx 0$ ), we can control  $E_{C_2}$  by roughly controlling  $|\rho_{14}|$ . Third, from Eq. (A4) we can rewrite

$$\rho_{22} \rho_{33} = \frac{E_{C_2}^2 + 4 |\rho_{14}| (|\rho_{14}| - E_{C_2})}{4}. \quad (16)$$

Then, by setting in the above equation  $\rho_{22} \rho_{33} \approx 0$  and  $E_{C_2}(\tau) = S(\tau)$  [here we again assume as our goal trajectory  $S(\tau)$  of Eq. (15)], we find an approximate value for  $|\rho_{14}| \approx \overline{|\rho_{14}|}$  which would lead to the tracking QC of  $E_C$ .

Since from the above we must have  $\rho_{11}(\tau) + \rho_{44}(\tau)$  close to one and given that we already start with  $\rho_{44}(0) = 1$ , the easier strategy is to keep  $\rho_{44}(\tau) \approx 1$ . So, employing the PTIQCM the control strategy is implemented as the following. At each  $\tau = \tau_m$  we look for a set of parameter values of the external

field such that  $|\rho_{14}(\tau)|$  is around  $\overline{|\rho_{14}(\tau)|}$  and  $\rho_{44}(\tau) \approx 1$ . Thus, we pick those for which  $|S(\tau) - E_{C_2}|$  is minimal. Moreover, we always check if indeed  $E_{C_2} \geq E_{C_1}$  (for extra technical details, see Ref. [54]).

Before presenting the results, we note that the exact type of noise constitutes a fundamental factor for the QC. In special, pure dephasing (PD) is the most difficult situation, so that conceivably we may be able to increase  $E_C$ , but only very slowly. On the other hand, the AD is far more easy to handle. A compromise emerges by adding AD to PD, the APD noise. This would be a way to create concurrence—by means of tracking QC—whenever the presence of PD is unavoidable in a given system [68].

In the examples, next we show the increasing of the concurrence by controlling the  $\rho_{jk}(\tau)$ 's (as described above) so

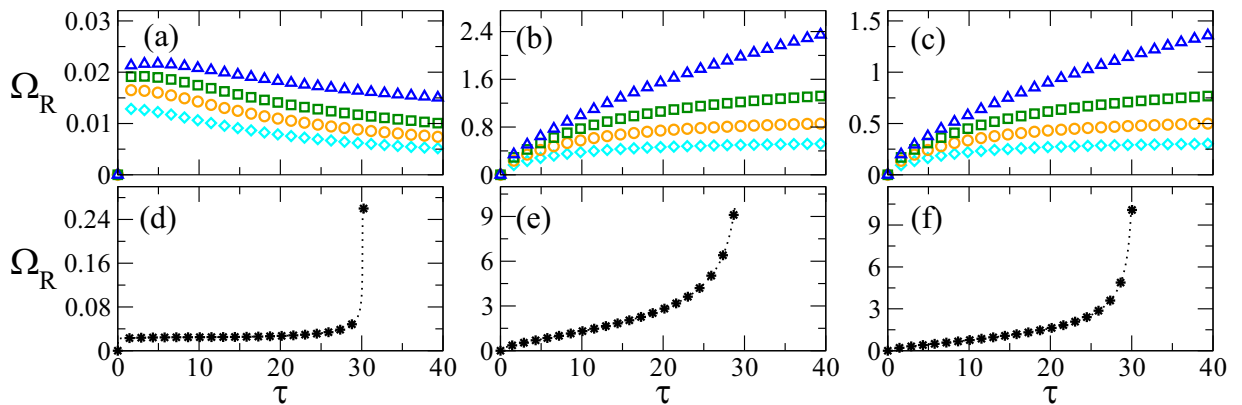


FIG. 8. External field amplitude profiles for the QC in Fig. 6. The symbols represent the values of  $S_0$ : 0.08 (diamond), 0.16 (circle), 0.24 (square), 0.32 (triangle), and 0.40 (star). [(a)–(c)] The cases in which the control is possible along the full time range  $0 \leq \tau \leq 40$ . [(d)–(f)] The situations where the control breaks down around  $\tau = 30$ . The PD, AD, and APD noise cases are displayed, respectively, in the first, second, and third columns.

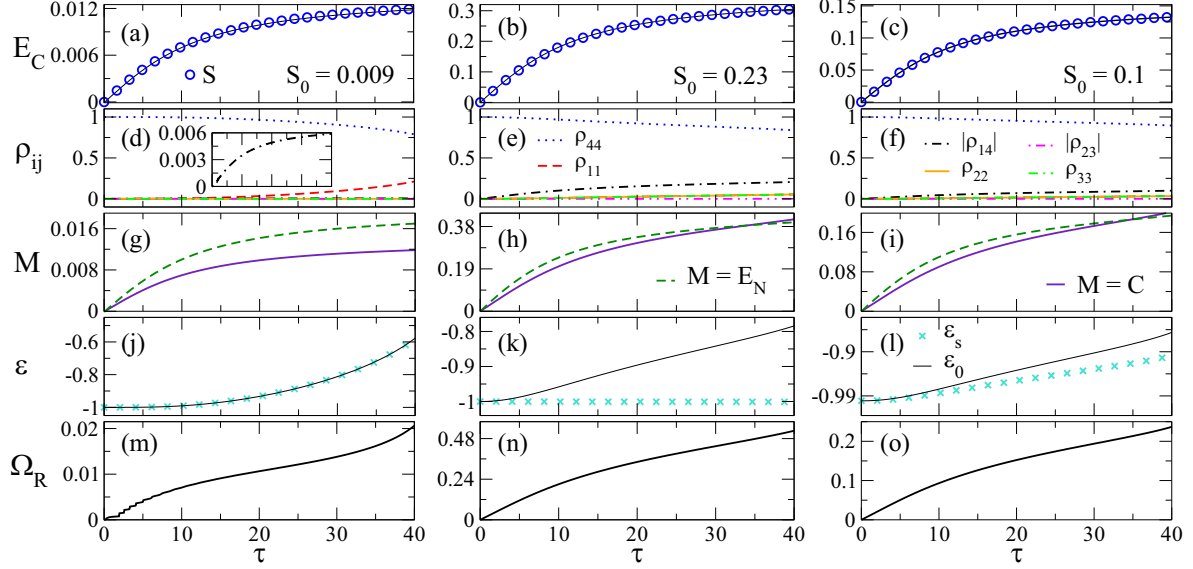


FIG. 9. [(a)–(c)] The obtained tracking QC of  $E_C$  (continuous line) following the target trajectory in Eq. (15) (circles). In the first, second, and third columns one has, respectively, PD and  $S_0 = 0.009$ , AD and  $S_0 = 0.23$ , and APD and  $S_0 = 0.10$ . [(d)–(f)] The associated  $\rho_{jk}$ 's. In panel (d), the inset shows  $|\rho_{14}|$ . The corresponding  $E_N$  and  $C$  are displayed in panels (g)–(i) and the energies  $\varepsilon_s$  and  $\varepsilon_0$  in panels (j)–(l). [(m)–(o)] The applied field amplitude profiles leading to the observed control.

to have  $E_C(\tau) = S(\tau)$ . The obtained  $E_C$ 's are depicted in Figs. 9(a)–9(c), respectively, for PD, AD, and APD. For PD, the QC is possible only for a very low  $S_0$  [cf., Eq. (15)],  $S_0 = 0.009$ . For AD, we can set a larger  $S_0 = 0.23$ . The intermediary case is APD, for which  $S_0 = 0.1$ . These values are close to the maximum possible  $S_0$ 's in  $S(\tau)$ , which still allow the QC for each type of noise (see below). At  $\tau = 40$ , the achieved concurrence is 0.012 for PD, 0.305 for AD, and 0.132 for APD. The calculated  $\rho_{jk}$ 's are displayed in Figs. 9(d)–9(f). Observe that the general trends for the density matrix elements here are not much distinct from those found for the population control.

As for the values of coherence and negativity, a positive side effect of the  $E_C$  control is that in all the noise cases, both  $C$  and  $E_N$  also increase; see Figs. 9(g)–9(h). Such behavior strongly contrasts with the “free” evolution seen in Figs. 3–5 and 7. The energies  $\varepsilon_s(\tau)$  and  $\varepsilon_0(\tau)$  are shown in Figs. 9(j)–9(l). The observed patterns are easy to understand with the help of Eqs. (8) and (9). For instance, as in some previous examples,  $\rho_{23}$  is null for all the noises. Consequently, once for PD  $\rho_{14}(\tau)$  is rather small [inset of Fig. 9 (d)],  $\varepsilon_s(\tau)$  and  $\varepsilon_0(\tau)$  are practically the same, as seen in Fig. 9(j). Moreover, even for a changing applied field, for the AD noise there is a fine-tuning combination of the terms leading to  $\varepsilon_s$ , such that similar to  $\varepsilon_s(\tau)$  in Figs. 4 and 6 the system energy expected value does not vary with time, i.e.,  $\varepsilon_s(\tau) = -1$ . The field amplitudes necessary for the QC are presented in Figs. 9(m)–9(o). They display smooth profiles.

As previously mentioned, to demand a very high increase of  $E_C$  can result in an earlier loss of QC. For the PD, we give an example in Fig. 10(a), where we compare the control in Fig. 9(a) with the same situation, but doubling the value of  $S_0$ . Although in the first case the QC is possible for  $\tau > 40$  (at  $\tau = 40$ ,  $E_C = 0.012$ ), in the second the control breaks down for  $\tau \approx 18$  (at which  $E_C \approx 0.02$ ). In Fig. 10(b), we have  $\varepsilon_0(\tau)$ .

We observe that the control is possible as long as  $\varepsilon_0$  is not too close to 0.

Given the above, one may ask if the control procedure could lead to a stabilization of entanglement, here  $E_C$ , for very long times (at least long enough for applications [69,70]). We notice that for our target trajectory  $S(\tau)$  in Eq. (15),  $S(\tau \rightarrow \infty) = \pi S_0/2$ , but for  $\tau \approx 10^3$  (with  $\gamma = 10$ ),  $S(t)$  already attains 99% of its maximum possible value. We have then considered our three types of noise, systematically changed  $S_0$ , and employed our QC method to test much longer times. For smaller values of  $S_0$  than those in Fig. 9, in Figs. 11(a)–11(c) we see that the QC can be sustained for times up to  $\tau = 10^3$ . Actually, we have considered even longer times (not shown here). For the PD, the control is lost around  $\tau = 1700$ , whereas for AD and APD, we have checked that up to  $\tau =$

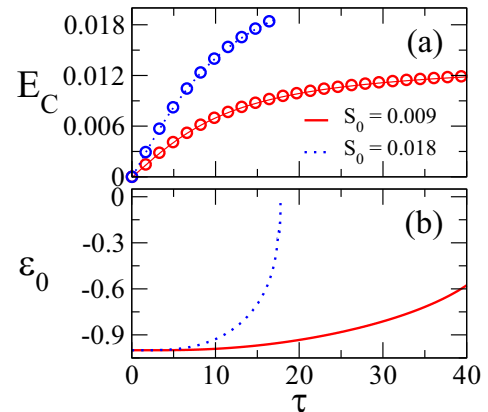


FIG. 10. (a) For the PD noise, comparison of the  $E_C$  tracking QC displayed in Fig. 9(a) ( $S_0 = 0.009$ ) with the case where  $S_0 = 0.018$ . In the latter, the control is lost around  $\tau \approx 18$ . (b) The behavior of  $\varepsilon_0(\tau)$ . The break down of the QC corresponds to  $\varepsilon_0$  approaching 0.

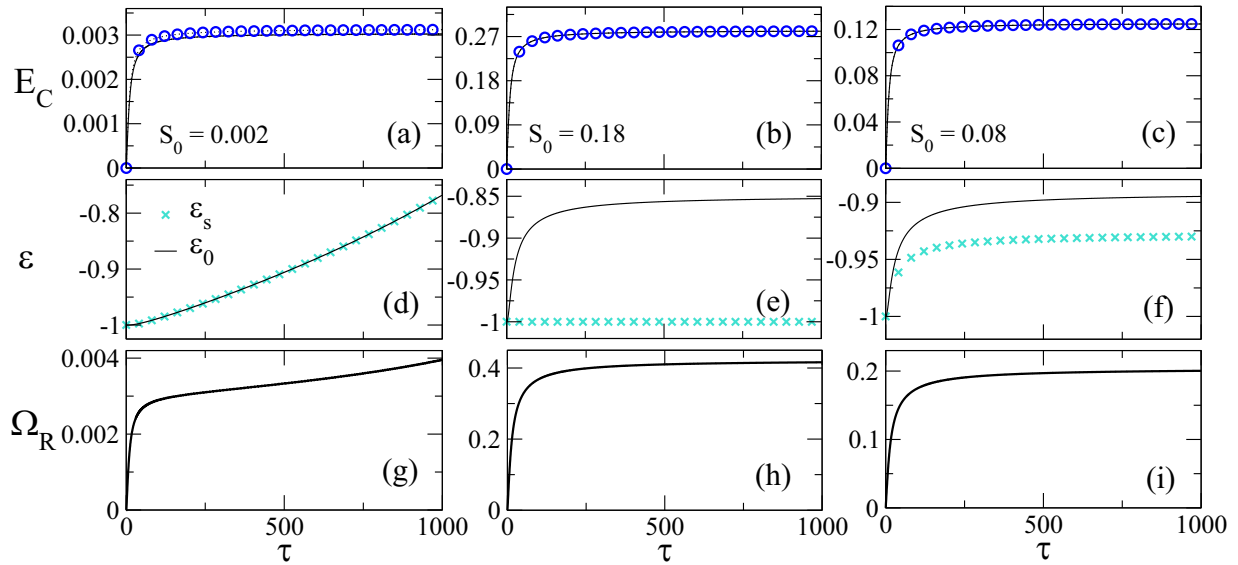


FIG. 11. The same QC as in Fig. 9, but for smaller  $S_0$ 's. The QC is maintained for much longer times, here up to  $\tau = 10^3$ . In the first, second, and third columns, one has, respectively, PD and  $S_0 = 0.002$ , AD and  $S_0 = 0.18$ , and APD and  $S_0 = 0.08$ .

3000, the tracking QC is still very stable. These trends eventually should be clear from the plots for the corresponding energies  $\varepsilon_0(\tau)$  and  $\varepsilon_s(\tau)$  in Figs. 11(d)–11(f) and applied field amplitudes  $\Omega_R(\tau)$  in Figs. 11(g)–11(i). Indeed, for PD the energies and the field amplitude increase much more quickly than  $E_C(\tau) = S(\tau)$  itself. This should asymptotically lead to a nonsustainable control process. In contrast, for AD and APD, we clearly have all the relevant physical quantities varying basically at the same pace, indicating an always tenable QC.

#### D. The trace distance during the quantum control

So far we have assumed that the two identical qubits interact equally with the environment, i.e.,  $\Gamma_1 = \Gamma_2 = \Gamma$ . We have found that the trace distance given by Eq. (A9) results in a null  $T_D$ —in fact, numerically always  $< 10^{-8}$ —for all our previously analyzed examples since in practice  $\rho_{22} = \rho_{33}$  in Figs. 1, 2, 4–6, and 9.

However, by assuming heterogeneous interactions of the qubits with the dissipative medium, namely,  $\Gamma_1 \neq \Gamma_2$ , conceivably we would have  $T_D \neq 0$ . Many applications in the realm of quantum information requires high fidelity (see the Appendix), so that  $T_D$  should be very close to zero. For instance, this is the case for the construction of efficient quantum logic gates, demanding a fidelity higher than 99.99% [71,72], and reliable protocols for quantum information transmission, for which the fidelity must be at least the astonishing 99.9994% [73]. These are very challenging goals for control methods (especially if based on the optimization of functionals): One must be able to manipulate the qubits and maintain them as similar as possible [49,74].

To unveil how our QC scheme can influence the system trace distance measure  $T_D$ , next we consider distinct  $\Gamma_1$  and  $\Gamma_2$ . In other words, we assume the qubits experiencing different degrees of dissipation from the environment. As a first test, we set  $\Gamma_1 = 0.1$  and vary  $0 < \Gamma_2 < 2\Gamma_1$ , supposing a

representative fixed external applied field of parameters  $\varphi = 0$  and  $\Omega_R = 0.5$  (for other values used in this work, the results are similar). A 2D density plot of  $T_D$  is shown in Fig. 12 for both the AD and APD noises. According to Eq. (A9), the trace distance depends only on the main diagonal terms of  $\rho$ , not affected by PD if it is the only type of noise in the environment. From Fig. 12 we see that for each  $\Gamma_2$ ,  $T_D$  as function of time oscillates. Nevertheless,  $T_D$  is always very small. In this way, the fidelity of the system with a heterogeneous coupling is

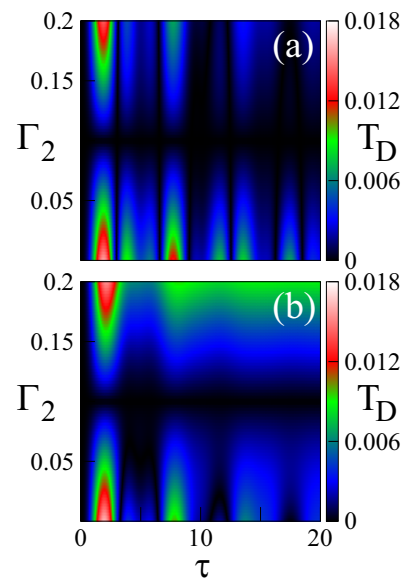


FIG. 12. The trace distance  $T_D$ , Eq. (A9), as function of  $\Gamma_2$  and time for an applied field with  $\varphi = 0$  and  $\Omega_R = 0.5$ . Here  $\Gamma_1 = 0.1$ . The system under the AD noise (a) and APD (b). The graphs are limited to the range  $0 \leq \tau \leq 20$  just for a better visualization. The overall pattern remains the same for larger times.

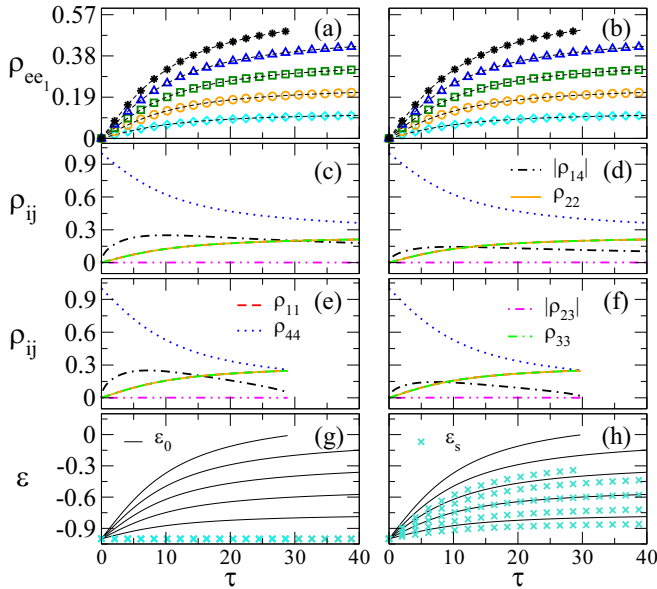


FIG. 13. [(a), (b)] The same QC and parameters of Figs. 6(b) and 6(c), but for  $\varphi = -\pi/2$  (see the main text) and a heterogeneous coupling of the qubits to the environment, where  $\Gamma_1 = 0.1$  and  $\Gamma_2 = 0.07$  (in Fig. 6,  $\Gamma_1 = \Gamma_2 = 0.1$ ). The left (right) column corresponds to the AD (APD) noise. The corresponding  $\rho_{jk}(t)$  for  $S_0 = 0.32$  in panels (c) and (d) and for  $S_0 = 0.4$  in panels (e) and (f). All the energies corresponding to panels (a) and (b) are given in panels (g) and (h).

kept considerably high, even with the application of a constant field.

Second, we repeat the population tracking QC of Fig. 6, but change the dissipation constant values. That for  $Q_1$  is retained,  $\Gamma_1 = 0.1$ , but now  $\Gamma_2 = 0.07$  for  $Q_2$ . We mention that  $\Gamma_1 = 0.07$  and  $\Gamma_2 = 0.1$  yields essentially the same qualitative behavior. Nonetheless, often the QC is easier to implement (e.g., through smoother fields) if the external potential is acting on the qubit of larger  $\Gamma$ . Before presenting the results, we shall comment on a relevant technical point. In all our previous analysis, for any time window  $m$  we have set  $\varphi_m = \varphi = 0$ , always getting a very good QC. For the present case of  $\Delta\Gamma \neq 0$ , such null phase also leads to a quite accurate population control (although the search for the field solutions is a bit more difficult and numerically more instable). Furthermore, it does not lead to the minimal possible profile for  $T_D(\tau)$ . Thus, we have tested different fixed  $\varphi$ 's and found that the best one to enforce high fidelity is  $\varphi = -\pi/2$ . The obtained QC in this case is depicted in Fig. 13.

Analogously to Fig. 6, the agreement between  $S(t)$  and  $\rho_{ee_1}(t)$  in Fig. 13 is remarkable; see Figs. 13(a)–13(c). Further, the control is also possible in the full range  $0 \leq \tau \leq 40$ , with the exception of  $S_0 = 0.4$ , when the QC breaks down for  $\tau \approx 30$ . In Figs. 13(c) and 13(d) [Figs. 13(e) and 13(f)], we display the matrix elements  $\rho_{jk}(\tau)$  for  $S_0 = 0.32$  ( $S_0 = 0.4$ ). Despite the fact that  $\Gamma_2$  is distinct in Figs. 6 and 13 (differing by 30%), the evolution of the  $\rho_{ij}$ 's as well as those of  $\varepsilon_0$  and  $\varepsilon_s$  are very similar in both cases. This should be expected since the goal trajectory and the initial state are exactly the same, and consequently they demand akin  $\rho(\tau)$ .

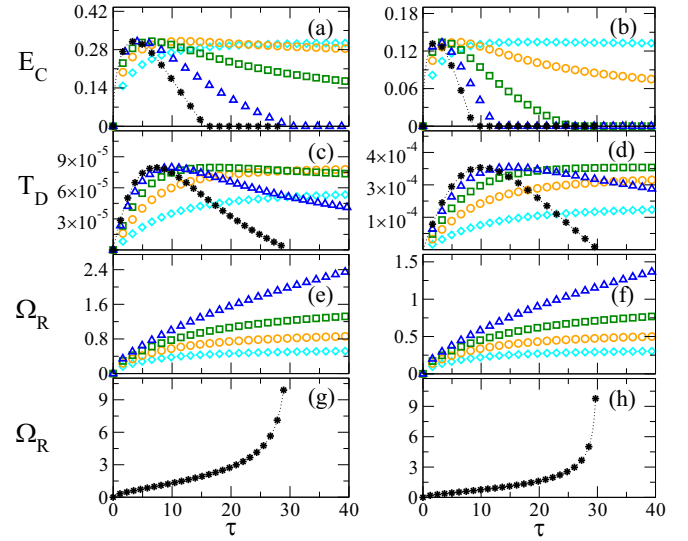


FIG. 14. The resulting  $E_C$  [(a), (b)] and  $T_D$  [(c), (d)] and the necessary external field amplitude profiles [(e)–(h)] for the QC of Fig. 13. The symbols represent the values of  $S_0$ : 0.08 (diamond), 0.16 (circle), 0.24 (square), 0.32 (triangle), and 0.40 (star). Similarly to the example in Fig. 6, for  $S_0 = 0.4$  the control is attained only up to  $\tau = 30$ . The left (right) column corresponds to the AD (APD) noise. Clearly,  $T_D$  is smaller for the AD than for the APD noise.

For the tracking QC of Fig. 13, the associated time evolution of  $E_C$  and  $T_D$  and the necessary field amplitude  $\Omega_R$  are depicted in Fig. 14. Comparing the  $E_C(\tau)$  plots in Figs. 7(b) and 7(c) with those in Figs. 14(a) and 14(b), we see that again they display essentially the exact same trends. In Figs. 14(c) and 14(d), we have the trace distance  $T_D(\tau)$ . Overall  $T_D$  presents rather small amplitudes for AD—for instance, even for the highest values observed, it is still amenable for the applications discussed in Refs. [71,72]—but somewhat more considerable for APD. Interestingly, for both AD and APD, after reaching a maximum at a certain  $\tau$  (which depends on  $S_0$ ),  $T_D$  tends to decrease more rapidly if  $S_0$  is larger. Note that such a fast decay of  $T_D$  with  $S_0$  is in parallel with the fact that  $\Omega_R(\tau)$  also increases faster for greater  $S_0$ 's, a behavior inferred from Figs. 14(e)–14(h).

As a last remark, by confronting the corresponding curves  $\Omega_R(\tau)$  in Figs. 8 and 14, one finds almost the same values. In fact, the typical difference is of only 0.3%. This indicates two general tendencies. First, changing the field phase  $\varphi$  may help to stabilize the numerical protocol but does not alter significantly the necessary amplitudes to achieve the control. Second, provided  $\Delta\Gamma$  is not too big (for the present set of parameters, we have determined the condition  $\Delta\Gamma < 0.04$ ) then  $\Omega_R$  is basically specified by the largest  $\Gamma_n$ .

## V. DISCUSSION AND CONCLUSION

In this contribution, we have considered a very simple, yet rather effective, tracking QC protocol, the PTQCM, to drive either population or entanglement of an open quantum system constituted by two coupled qubits ( $Q_1$  and  $Q_2$ ). For the system evolving as a  $X$  state and for the  $Q_n$ 's subjected

to a dissipative environment, the control is attained by means of a piecewise time-independent tunable electric field, whose scaled amplitude  $\Omega_R$  is properly set at time intervals  $\delta t$ .

During the control, the energy expected value of the qubits ( $\varepsilon_0$ ) and of the  $Q_n$ 's plus field ( $\varepsilon_s$ ), as well as quantities like coherence, concurrence, negativity, and trace distance (this last closely related to fidelity) have been monitored. As for the noise types; we have addressed phase damping (PD), which inflicts a decay to the off-diagonal terms of  $\rho$ ; amplitude damping (AP), which mediates an energy flux from the system to the medium, mainly by acting on the density matrix diagonal terms  $\rho_{jj}$ ; and a mixture of both, called the amplitude phase damping (APD).

By collecting all the obtained results in this contribution, some prospects on the behavior of (two) coupled qubits in a noise environment can be summarized as the following.

The PD is more frequently associated to loss of quantum coherence [52], but indirectly it also may cause energy drain or even gain if there is an external applied field to the system (for a discussion about the eventual associated mechanisms; see, e.g., Refs. [54,75]). The key factor is that under the PD noise, the system natural behavior is to set to zero the off-diagonal terms of  $\rho(t)$ . Thus, the PD noise constitutes a great challenge if one needs to create quantum information resources, i.e., coherence and entanglement. On the other hand, the energy damping is usually strong for the AD. Nevertheless, if a simple constant field is applied, some degree of entanglement and coherence is preserved in the system (refer to Figs. 4 and 5).

By implementing the population tracking QC (Fig. 6), the measures  $C$  and  $E$  tend to zero with time for PD. However, they can be maintained to reasonable values for AD, provided the goal trajectory  $S(t)$  does not vary too fast, i.e., if  $S_0$  is not too high in Eq. (15) (Fig. 7). Interestingly, if we add AD to the PD noise (the APD), the mentioned coherence and entanglement measures become those of the AD case. The price is that the typical fields amplitudes for the QC are relatively higher for AD and APD than for PD (Fig. 8). These findings corroborate the idea of *combating noise with noise* [68], proposed in the context of quantum teleportation. If somehow the PD noise is ubiquitous in a particular medium—as in certain experimental realizations of quantum memories and quantum networks [76–78]—the introduction of AD can be beneficial as it concerns entanglement preservation, made possible through QC; compare Figs. 7(a), 7(d) and 7(g) with Figs. 7(c), 7(f) and 7(i).

We have likewise considered tracking QC to directly drive entanglement, here the concurrence measure  $E_C$  (Fig. 9). There is a great difference between the possible maximum values achieved for  $E_C$  under PD or AD. Hence, compromise values can be obtained by adding AD to the PD noise. Indeed, see Figs. 9(a)–9(c) and Figs. 11(a)–11(c) and also Fig. 10. Further, although in our examples the goal was to control  $E_C$ , as a positive side-effect both the negativity  $E_N$  and the coherence  $C$  have similarly increased in the system. Perhaps equally important is the fact that such control can be sustained for very long times (Fig. 10). We should emphasize that from a practical point of view, maintaining entanglement for long periods is essential for the reliability of quantum information devices [6] as well as to assure security in quantum key dis-

tribution, fidelity in quantum communication protocols, and robustness of quantum state storage [16,50]. Also of note is that the tracking QC of  $E_C$  demands field amplitudes  $\Omega_R$  which are much lower than those necessary to perform the population control (Figs. 8, 9, and 11).

A low trace distance  $T_D$  (associated to high fidelity) is necessary in many potential usages of entanglement as a resource for quantum information processing. Relevant illustrations are quantum memories [79] and quantum communication devices [80]. We have clearly met this condition for our examples in which  $\Gamma_1 = \Gamma_2$ , getting  $T_D = 0$  during the whole QC process. For all the instances of  $\Gamma_1 \neq \Gamma_2$  we have investigated—Figs. 13 and 14 illustrate a typical situation—the tracking control has always been achieved with very good precision. However,  $T_D$  can be different from zero, either presenting a plateau-like behavior or displaying a peak that fades away as  $\tau$  increases. Despite that,  $T_D$  is kept small for the AD noise, thus presumably not a serious problem in applications. For the APD, the variation of  $T_D$  becomes more appreciable.

Throughout this work, we have considered noises which are Markovian in nature and thus can be described by the Lindblad operator. But non-Markovian thermal noise usually has significant influence on the evolution of a quantum system when the temperature is not too low, obviously influencing the system entanglement. An important query is then to determine how thermal noise would affect our present results. One should consider our control protocol together with frameworks like the hierarchical equations of motion (HEOM) theory (see, e.g., Refs. [81–83]). We hope this is going to be addressed in the near future.

Next, we briefly remark on the eventual practical implications of our present study. Often, quantum information protocols are discussed assuming qubits very close to perfect isolation. This is the case, e.g., for  $Q_n$ 's based on superconductors [84,85] or trapped ions [86–88] setups. For these constructions, the environmental influence can be reduced to a minimum. Thus, operations like full population inversion are possible. Also, entanglement can reach very high values. Nonetheless, such examples are of course experimentally very difficult to implement. Because of that, it is also relevant to investigate less technologically demanding realizations for qubits, consequently undergoing stronger coupling with the environment. As a consequence, there are greater limitations in the type of quantum “engineering” one may be able to execute (even for a single qubit; see Refs. [35–37]). However, they still may be useful for quantum computation. As an illustration, we cite analysis involving the quantum computer IBM-QX5, for which the degree of entanglement between any two pairs of qubits (in a total of 16) is not particularly high—refer to Ref. [5]. We mention that just to test these limits, we have assumed on purpose relatively large values for the  $\Gamma$ 's in the present work. Moreover, for the particular instances in which the QC has been lost [e.g., those cases associated to rapidly increasing tracking trajectories  $S(\tau)$ ], the breakdowns were not due to the particular protocol, PTIQCM, we have used. Indeed, from the energetic balance analysis, we have clearly demonstrated that the problem is associated to the very physical nature of the interaction with the environment and how such interaction dissipates energy and washes out coherence, destroying quantum interference. These are important

aspects to be taken into account in actual quantum information tasks.

Finally, we have considered two qubits,  $N = 2$ . The study of larger  $N$ 's often requires much more sophisticated protocols. Indeed, as the number of qubits increases linearly, the number of levels in the density matrix grows exponentially. We believe that our present approach allied with schemes like scalable machine learning [89] and/or gradient ascent pulse engineering (GRAPE) [90] would represent a proper way to deal with a greater collection of  $Q_n$ 's. This will be the topic of a forthcoming contribution.

### ACKNOWLEDGMENTS

G.J.D. (405240/2018-0) and M.G.E.d.L. (304532/2019-3) acknowledge CNPq for research grants and A.L.O.d.S. would like to thank CAPES for a Ph.D. scholarship.

### APPENDIX: SOME MEASURES FOR QUANTUM COHERENCE AND ENTANGLEMENT

There are different ways to characterize the degree of entanglement of a system. Each possible measure might be useful to unveil a distinct physical aspect of the problem [13]. The same is true regarding quantum coherence [15,51]. Below we describe the definitions we use in the present work.

#### 1. Coherence

Due to the special configuration of  $X$  states, Eq. (7), partial traces do not constitute the most appropriate protocol to quantify the system ‘‘amount’’ of coherence [15]. Instead, one should deal with the full composed system. Thus, a possible measure is that of the  $l_1$  norm [91], or

$$C = \sum_{\substack{j,k \\ j \neq k}} |\rho_{jk}|. \quad (\text{A1})$$

This is perhaps the simplest assessment of coherence and the one we employ in our analysis.

#### 2. Entanglement

There are many alternative measures for entanglement. We list a few of the most commonly addressed in the literature and which are used in the present work.

*Concurrence.* For bipartite systems, concurrence is often considered due to its close relation to the idea of *entanglement of formation* (see, e.g., Ref. [53]). For two qubits of density matrix  $\rho$ , the spin-flipped operator  $\tilde{\rho}$  reads (with \* meaning complex conjugation)

$$\tilde{\rho} = (\sigma_y \otimes \sigma_y) \rho^* (\sigma_y \otimes \sigma_y). \quad (\text{A2})$$

Then, the concurrence follows from

$$E_C(\rho) = \text{Max}(\sqrt{\lambda_1} - \sqrt{\lambda_2} - \sqrt{\lambda_3} - \sqrt{\lambda_4}, 0), \quad (\text{A3})$$

with  $\lambda_1 \geq \lambda_2 \geq \lambda_3 \geq \lambda_4$  being the eigenvalues of  $\rho \tilde{\rho}$ . One has that  $0 \leq E_C(\rho) \leq 1$ , with 1 representing maximal

entanglement. Moreover, in our case we can write [62]

$$\begin{aligned} E_C(\rho) &= \text{Max}(0, E_{C_1}, E_{C_2}), \quad E_{C_1} = 2(\sqrt{\rho_{23}\rho_{32}} - \sqrt{\rho_{11}\rho_{44}}), \\ E_{C_2} &= 2(\sqrt{\rho_{14}\rho_{41}} - \sqrt{\rho_{22}\rho_{33}}). \end{aligned} \quad (\text{A4})$$

A scheme to control concurrence has been described in Ref. [54]. The idea is the following [hereafter, for  $n$  indicating qubit 1 (2),  $\bar{n}$  indicates qubit 2 (1)]. One determines from the initial state which  $E_{C_n}$  is greater at  $t = 0$ . Suppose it is  $E_{C_{\bar{n}}}$ . Then, for the goal being to increase the concurrence (the target path  $S(t) > 0$  is an increasing function of time), we just control the density matrix elements, according to Eq. (A4), so to make  $E_{C_{\bar{n}}} = S(t)$  (we have found from exhaustive numerical tests that whenever  $E_{C_{\bar{n}}}$  increases,  $E_{C_n}$  tends to decrease, so the Max condition in Eq. (A4) is always satisfied by  $E_{C_{\bar{n}}}$ ).

*Negativity.* Another important concept is that of negativity [92]. One of its features is that the negativity of  $\rho$ ,  $N(\rho)$ , does not increase under LOCC (local operations and classical communication), resulting in a monotonic measure of entanglement.  $N(\rho)$  is defined as (for  $\rho^\dagger$  the Hermitian adjoint of  $\rho$ )

$$N(\rho) = \frac{1}{2}(\text{Tr}[\sqrt{\rho^\dagger \rho}] - 1). \quad (\text{A5})$$

Then, one can define the logarithmic negativity (a measure of entanglement) by

$$E_N(\rho) = \log_2 [2N(\rho) + 1], \quad (\text{A6})$$

which establishes an upper bound to the possible distillable entanglement of  $\rho(t)$  [92,93].

Since both concurrence and (logarithmic) negativity are defined in the same interval range,  $0 \leq E \leq 1$ , it makes sense to compare them for a given system. In fact, they yield exactly the same numerical values for pure states [13,94].

*Trace distance.* Quantum memory effects can be quantified through the trace distance  $T_D$  between two arbitrary quantum states  $\rho_a$  and  $\rho_b$ , or [15]

$$T_D(\rho_a, \rho_b) = \frac{1}{2} \text{Tr}[|\rho_a - \rho_b|]. \quad (\text{A7})$$

Moreover,  $\text{Tr}(\rho_a, \rho_b)$  is related to the fidelity (or ‘‘closeness’’) between  $\rho_a$  and  $\rho_b$  [95]. Actually, the fidelity  $0 \leq F(\rho_a, \rho_b) \leq 1$  has the lower bound

$$F(\rho_a, \rho_b) \geq 1 - T_D(\rho_a, \rho_b). \quad (\text{A8})$$

A composite open quantum system under the action of Markovian processes generally goes through a flux of information from it to the environment. However, the information loss may be distinct for each system part. To gauge how this takes place for our two-qubit case, the previous  $\rho_a$  and  $\rho_b$  in Eq. (A7) can be taken as the reduced density matrices of the corresponding subsystems. So, for our present problem [cf. Eq. (7)]

$$T_D(\rho_{\bar{1}}, \rho_{\bar{2}}) = |\rho_{22} - \rho_{33}|, \quad (\text{A9})$$

where  $\rho_{\bar{n}} = \text{Tr}_n(\rho)$ , with  $\text{Tr}_n$  being the partial trace over the variables of  $Q_n$ .

- [1] J. Hu and H. Yu, *Phys. Rev. A* **91**, 012327 (2015).
- [2] J. G. Richens, J. H. Selby, and S. W. Al-Safi, *Phys. Rev. Lett.* **119**, 080503 (2017).
- [3] S. K. Goyal, S. Banerjee, and S. Ghosh, *Phys. Rev. A* **85**, 012327 (2012).
- [4] L. Aolita, F. de Melo, and L. Davidovich, *Rep. Prog. Phys.* **78**, 042001 (2015).
- [5] Y. Wang, Y. Li, Z.-Q. Yin, and B. Zeng, *npj Quantum Inf.* **4**, 46 (2018).
- [6] C. Bény, C. T. Chubb, T. Farrelly, and T. J. Osborne, *Nat. Commun.* **9**, 3792 (2018).
- [7] M. Ghasemi and M. K. Tavassoly, *Quantum Inf. Process.* **18**, 113 (2019).
- [8] L. Gyongyosi and S. Imre, *Quantum Inf. Process.* **18**, 107 (2019).
- [9] K. Hou, D. Q. Bao, C. J. Zhu, and Y. P. Yang, *Quantum Inf. Process.* **18**, 104 (2019).
- [10] J. T. Barreiro, *Nat. Phys.* **7**, 927 (2011).
- [11] C. Kiefer and E. Joos, in *Quantum Future from Volta and Como to the Present and Beyond* (Springer, Berlin, 1999).
- [12] F. Galve and E. Lutz, *Phys. Rev. A* **79**, 032327 (2009).
- [13] R. Horodecki, P. Horodecki, M. Horodecki, and K. Horodecki, *Rev. Mod. Phys.* **81**, 865 (2009).
- [14] C. Brif, R. Chakrabarti, and H. Rabitz, *New J. Phys.* **12**, 075008 (2010).
- [15] B. H. Liu, L. Li, Y. F. Huang, C. F. Li, G. C. Guo, E. M. Laine, H. P. Breuer, and J. Piilo, *Nat. Phys.* **7**, 931 (2011).
- [16] R. Lo Franco, A. D'Arrigo, G. Falci, G. Compagno, and E. Paladino, *Phys. Rev. B* **90**, 054304 (2014).
- [17] E. Paladino, Y. M. Galperin, G. Falci, and B. L. Altshuler, *Rev. Mod. Phys.* **86**, 361 (2014).
- [18] M. H. M. Passos, W. F. Balthazar, A. Z. Khoury, H. Hor-Meyll, L. Davidovich, and J. A. O. Huguenin, *Phys. Rev. A* **97**, 022321 (2018).
- [19] S. R. Beane, D. B. Kaplan, N. Klco, and M. J. Savage, *Phys. Rev. Lett.* **122**, 102001 (2019).
- [20] F. Gao, R. Rey-de-Castro, Y. Wang, H. Rabitz, and F. Shuang, *Phys. Rev. A* **93**, 053407 (2016).
- [21] Z. Xi, Y. Li, and H. Fan, *Sci. Rep.* **5**, 10922 (2015).
- [22] A. R. R. Carvalho and J. J. Hope, *Phys. Rev. A* **76**, 010301(R) (2007).
- [23] A. R. R. Carvalho, A. J. S. Reid, and J. J. Hope, *Phys. Rev. A* **78**, 012334 (2008).
- [24] S. Maniscalco, F. Francica, R. L. Zaffino, N. Lo Gullo, and F. Plastina, *Phys. Rev. Lett.* **100**, 090503 (2008).
- [25] Y. Lin, J. P. Gaebler, F. Reiter, T. R. Tan, R. Bowler, A. S. Sorensen, D. Leibfried, and D. J. Wineland, *Nature (London)* **504**, 415 (2013).
- [26] S. Shankar, M. Hatridge, Z. Leghtas, K. M. Sliwa, A. Narla, U. Vool, S. M. Girvin, L. Frunzio, M. Mirrahimi, and M. H. Devoret, *Nature (London)* **504**, 419 (2013).
- [27] G. H. Aguilar, A. Valdes-Hernandez, L. Davidovich, S. P. Walborn, and P. H. Souto Ribeiro, *Phys. Rev. Lett.* **113**, 240501 (2014).
- [28] F. Dolde, V. Bergholm, Y. Wang, I. Jakobi, B. Naydenov, S. Pezzagna, J. Meijer, F. Jelezko, P. Neumann, T. S. Herbrüggen, J. Biamonte, and J. Wrachtrup, *Nat. Commun.* **5**, 3371 (2014).
- [29] C. Gonzalez-Ballester, E. Moreno, and F. J. G. Vidal, *Phys. Rev. A* **89**, 042328 (2014).
- [30] W. B. Gao, A. Imamoglu, H. Bernien, and R. Hanson, *Nat. Photon.* **9**, 363 (2015).
- [31] Z. Man, Y. Xia, and R. L. Franco, *Sci. Rep.* **5**, 13843 (2015).
- [32] M. Rafiee, A. Nourmandipour, and S. Mancini, *Phys. Rev. A* **94**, 012310 (2016).
- [33] M. Rafiee, A. Nourmandipour, and S. Mancini, *Phys. Rev. A* **96**, 012340 (2017).
- [34] M. Rafiee, A. Nourmandipour, and S. Mancini, *Phys. Lett. A* **384**, 126748 (2020).
- [35] I. Medina and F. L. Semião, *Phys. Rev. A* **100**, 012103 (2019).
- [36] D. Ran, W.-J. Shan, Z.-C. Shi, Z.-B. Yang, J. Song, and Y. Xia, *Phys. Rev. A* **101**, 023822 (2020).
- [37] D. Ran, B. Zhang, Y.-H. Chen, Z.-C. Shi, Y. Xia, R. Ianculescu, J. Scheuer, and A. Gover, *Opt. Lett.* **45**, 3597 (2020).
- [38] G. Chiribella and Y. Yang, *Phys. Rev. A* **96**, 022327 (2017).
- [39] J. H. Huang and S. Y. Zhu, *Phys. Rev. A* **76**, 062322 (2007).
- [40] J. T. Barreiro, M. Müller, P. Schindler, D. Nigg, T. Monz, M. Chwalla, M. Hennrich, C. F. Roos, P. Zoller, and R. Blatt, *Nature (London)* **470**, 486 (2011).
- [41] S. Campbell, F. Ciccarello, G. M. Palma, and B. Vacchini, *Phys. Rev. A* **98**, 012142 (2018).
- [42] S. Vinjanampathy and A. R. P. Rau, *Phys. Rev. A* **82**, 032336 (2010).
- [43] T. Yu and J. H. Eberly, *Science* **323**, 598 (2009).
- [44] H. M. Wiseman and G. J. Milburn, *Quantum Measurement and Control* (Cambridge University Press, Cambridge, UK, 2009).
- [45] J. Kuhn and M. G. E. da Luz, *Phys. Rev. A* **75**, 053410 (2007).
- [46] G. J. Delben and M. G. E. da Luz, *Quantum Inf. Process.* **15**, 1955-1978 (2016).
- [47] C. A. Estrada Guerra, D. V. Villamizar, and L. G. C. Rego, *Phys. Rev. A* **86**, 023411 (2012).
- [48] Y. C. Chang, J. Xing, F. H. Zhang, G. Q. Liu, Q. Q. Jiang, W. X. Li, C. Z. Gu, G. L. Long, and X. Y. Pan, *Appl. Phys. Lett.* **104**, 262403 (2014).
- [49] J. Randall, A. M. Lawrence, S. C. Webster, S. Weidt, N. V. Vitanov, and W. K. Hensinger, *Phys. Rev. A* **98**, 043414 (2018).
- [50] J. Jing, T. Yu, C. H. Lam, J. Q. You, and L. A. Wu, *Phys. Rev. A* **97**, 012104 (2018).
- [51] H. Breuer and F. Petruccione, *The Theory of Open Quantum Systems* (Oxford University Press, Oxford, UK, 2007).
- [52] M. A. Nielsen and I. L. Chuang, *Quantum Computation and Quantum Information* (Cambridge University Press, Cambridge, UK, 2000).
- [53] S. C. Hou, X. L. Huang, and X. X. Yi, *Phys. Rev. A* **82**, 012336 (2010).
- [54] G. J. Delben and M. W. Beims, *Phys. Scr.* **96**, 025102 (2021).
- [55] A.-B. A. Mohamed and H. Eleuch, *Sci. Rep.* **10**, 13240 (2020).
- [56] H. Brox, J. Bergli, and Y. M. Galperin, *J. Phys. A: Math. Theor.* **45**, 455302 (2012).
- [57] L.-A. Wu, C. X. Yu, and D. Segal, *New J. Phys.* **15**, 023044 (2013).
- [58] P. Szańkowski, M. Trippenbach, and L. Cywiński, *Phys. Rev. A* **94**, 012109 (2016).
- [59] T. Chatchawaltheerat, S. Khemmani, and J. Poulter, *Phys. Lett. A* **383**, 125882 (2019).
- [60] M. Cattaneo, G. L. Giorgi, S. Maniscalco, and R. Zambrini, *New J. Phys.* **21**, 113045 (2019).
- [61] D. Tiwari, S. Datta, S. Bhattacharya, and S. Banerjee, [arXiv:2205.04135](https://arxiv.org/abs/2205.04135).

- [62] M. Ikram, F. L. Li, and M. S. Zubairy, *Phys. Rev. A* **75**, 062336 (2007).
- [63] D. Girolami and G. Adesso, *Phys. Rev. A* **83**, 052108 (2011).
- [64] A. Singh, S. Pradyumna, A. R. P. Rau, and U. Sinha, *J. Opt. Soc. Am. B: Opt. Phys.* **34**, 681 (2017).
- [65] Z. Wang, J. Casanova, and M. B. Plenio, *Nat. Commun.* **8**, 14660 (2017).
- [66] A. L. O. dos Santos and G. J. Delben, *Phys. A (Amsterdam, Neth.)* **574**, 126017 (2021).
- [67] S. M. Hein, F. Schulze, A. Carmele, and A. Knorr, *Phys. Rev. A* **91**, 052321 (2015).
- [68] R. Fortes and G. Rigolin, *Phys. Rev. A* **92**, 012338 (2015).
- [69] S. N. Filippov and M. Ziman, *Phys. Rev. A* **90**, 010301(R) (2014).
- [70] J. Y. Zhou, Y. H. Zhou, X. L. Yin, J. F. Huang, and J. Q. Liao, *Sci. Rep.* **10**, 12557 (2020).
- [71] T. P. Harty, M. A. Sepiol, D. T. C. Allcock, C. J. Ballance, J. E. Tarlton, and D. M. Lucas, *Phys. Rev. Lett.* **117**, 140501 (2016).
- [72] R. J. Spiteri, M. Schmidt, J. Ghosh, E. Zahedinejad, and B. C. Sanders, *New J. Phys.* **20**, 113009 (2018).
- [73] P. Kaufmann, T. F. Gloger, D. Kaufmann, M. Johanning, and C. Wunderlich, *Phys. Rev. Lett.* **120**, 010501 (2018).
- [74] M. H. Goerz, K. B. Whaley, and C. P. Koch, *EPJ Quantum Technol.* **2**, 21 (2015).
- [75] Z. H. Wang, Y. J. Ji, Y. Li, and D. L. Zhou, *Phys. Rev. A* **91**, 013838 (2015).
- [76] B. Jing, X. J. Wang, Y. Yu, P. F. Sun, Y. Jiang, S. J. Yang, W. H. Jiang, X. Y. Luo, J. Zhang, X. Jiang, X. H. Bao, and J. W. Pan, *Nat. Photon.* **13**, 210 (2019).
- [77] P. C. Humphreys, N. Kalb, J. P. J. Morits, R. N. Schouten, R. F. L. Vermeulen, D. J. Twitchen, M. Markham, and R. Hanson, *Nature (London)* **558**, 268 (2018).
- [78] M. Pant, H. Krovi, D. Towsley, L. Tassiulas, L. Jiang, P. Basu, D. Englund, and S. Guha, *npj Quantum Inf.* **5**, 25 (2019).
- [79] S. Zaiser, T. Rendler, I. Jakobi, T. Wolf, S. Y. Lee, S. Wagner, V. Bergholm, T. S. Herbrüggen, P. Neumann, and J. Wrachtrup, *Nat. Commun.* **7**, 12279 (2016).
- [80] W. Zhang, D. S. Ding, Y. B. Sheng, L. Zhou, B. S. Shi, and G. C. Guo, *Phys. Rev. Lett.* **118**, 220501 (2017).
- [81] A. G. Dijkstra and Y. Tanimura, *Phys. Rev. Lett.* **104**, 250401 (2010).
- [82] A. Kato and Y. Tanimura, *J. Chem. Phys.* **143**, 064107 (2015).
- [83] P. P. Hofer, M. P. Llobet, L. D. M. Miranda, G. Haack, R. Silva, J. B. Brask, and N. Brunner, *New J. Phys.* **19**, 123037 (2017).
- [84] R. Barends, J. Kelly, A. Megrant, A. Veitia, D. Sank, E. Jeffrey, T. C. White, J. Mutus, A. G. Fowler, B. Campbell, Y. Chen, Z. Chen, B. Chiaro, A. Dunsworth, C. Neill, P. O'Malley, P. Roushan, A. Vainsencher, J. Wenner, A. N. Korotkov, and A. N. Cleland, and J. M. Martinis, *Nature (London)* **508**, 500 (2014).
- [85] D. K. Weiss, A. C. Y. Li, D. G. Ferguson, and J. Koch, *Phys. Rev. B* **100**, 224507 (2019).
- [86] T. Choi, S. Debnath, T. A. Manning, C. Figgatt, Z.-X. Gong, L.-M. Duan, and C. Monroe, *Phys. Rev. Lett.* **112**, 190502 (2014).
- [87] N. M. Linke, D. Maslov, M. Roetteler, S. Debnath, C. Figgatt, K. A. Landsman, and K. Wright, and C. Monroe, *Proc. Natl. Acad. Sci. USA* **114**, 3305 (2017).
- [88] P. H. Leung, K. A. Landsman, C. Figgatt, N. M. Linke, C. Monroe, and K. R. Brown, *Phys. Rev. Lett.* **120**, 020501 (2018).
- [89] J. Carrasquilla, G. Torlai, R. G. Melko, and L. Aolita, *Nat. Mach. Intell.* **1**, 155 (2019).
- [90] M. Abdelhafez, D. I. Schuster, and J. Koch, *Phys. Rev. A* **99**, 052327 (2019).
- [91] T. Baumgratz, M. Cramer, and M. B. Plenio, *Phys. Rev. Lett.* **113**, 140401 (2014).
- [92] G. Vidal and R. F. Werner, *Phys. Rev. A* **65**, 032314 (2002).
- [93] N. Friis, G. Vitagliano, M. Malik, and M. Huber, *Nat. Rev. Phys.* **1**, 72 (2019).
- [94] F. Verstraete, K. Audenaert, J. Dehaene, and B. D. Moor, *J. Phys. A: Math. Gen.* **34**, 10327 (2001).
- [95] R. Jozsa, *J. Mod. Opt.* **41**, 2315 (1994).